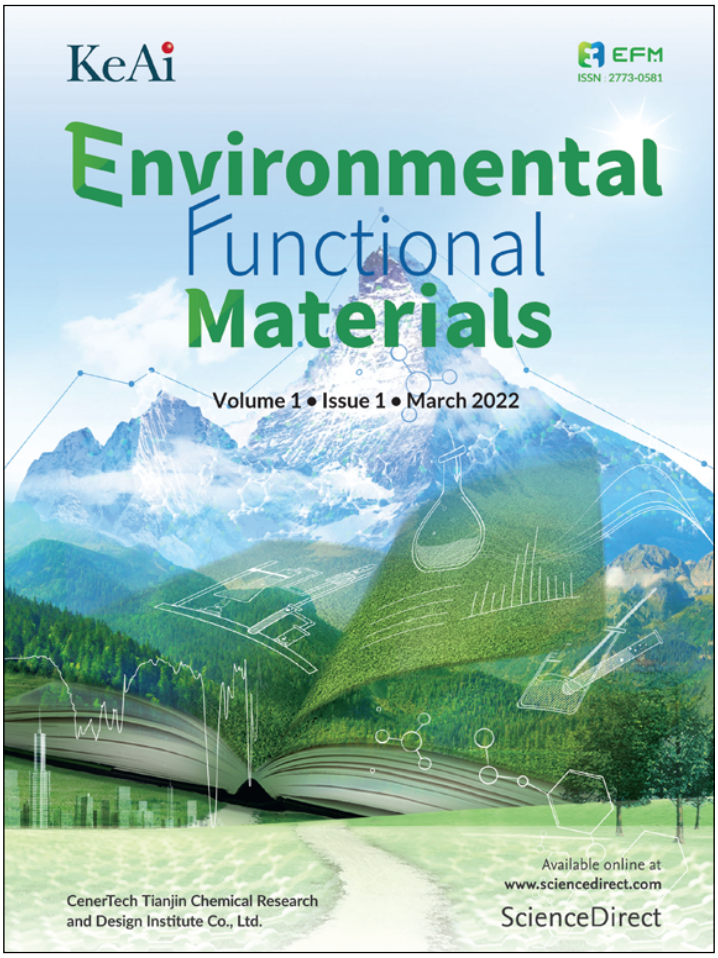

Environmental Functional Materials 1 (2022) 49–66

Contents lists available at ScienceDirect

Environmental Functional Materials

journal homepage: www.keaipublishing.com/en/journals/environmental-functional-materials

Light-response adsorption and desorption behaviors of metal–organic frameworks

Chao-Yang Wang [a], Lingshan Ma [b,c], Chong-Chen Wang [a,*], Peng Wang [a], Leonardo Gutierrez [b,c], Weiwei Zheng [d]

[a] Beijing Key Laboratory of Functional Materials for Building Structure and Environment Remediation/Beijing Energy Conservation & Sustainable Urban and Rural Development Provincial and Ministry Co-construction Collaboration Innovation Center, Beijing University of Civil Engineering and Architecture, Beijing, 100044, PR China
[b] Center for Microbial Ecology and Technology (CMET), Ghent University, Coupure Links 653, 9000, Ghent, Belgium
[c] Center for Advanced Process Technology for Urban Resource Recovery (CAPTURE), Frieda Saeysstraat 1, 9000, Ghent, Belgium
[d] Department of Chemistry, Syracuse University, Syracuse, NY, 13244, United States

HIGHLIGHTS

- The recent progresses of light-response MOFs were reviewed.
- The light-response adsorption/desorption in aqueous phase were discussed.
- The fabrication strategies of light-response MOFs were presented.
- The mechanisms of light-induced adsorption/desorption were summarized.
- The outlooks of the further development of light-response MOFs are proposed.

GRAPHICAL ABSTRACT

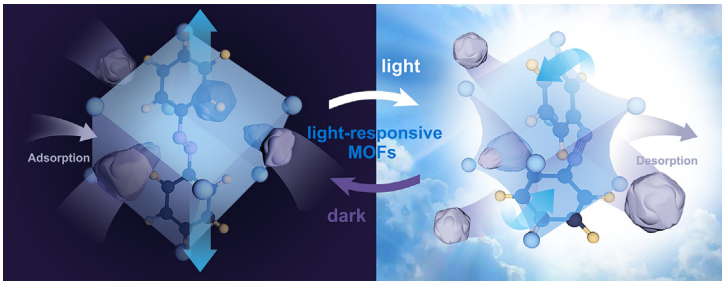

ARTICLE INFO

Keywords:
Light response
Metal–organic frameworks
Adsorption
Desorption
Mechanism

ABSTRACT

Metal–organic frameworks (MOFs) are ideal adsorbents because of their porous structure, ultra-large specific surface area, abundant active sites, and specific surface charge. Recently, light-response MOFs have received considerable research interests regarding their potential applications in environmental remediation, medical treatment, and artificial intelligence. This review systematically summarizes the recent progress of light-response MOFs and MOF-based composites for light-response adsorption/desorption. The fabrication strategies of light-response MOFs, including in situ synthesis, post-synthesis modification, and introduction of guest molecules, are presented. The mechanisms of light-induced structural change and light-responsive adsorption/desorption are summarized. The prospects for further development of light-response MOFs are discussed. The facile regeneration of light-response MOF-based adsorbents by light irradiation is highly promising for energy saving, environmental friendliness, and sustainability.

* Corresponding author. Beijing Key Laboratory of Functional Materials for Building Structure and Environment Remediation/Beijing Energy Conservation & Sustainable Urban and Rural Development Provincial and Ministry Co-construction Collaboration Innovation Center, Beijing University of Civil Engineering and Architecture, Beijing, 100044, PR China.
E-mail addresses: chongchenwang@126.com, wangchongchen@bucea.edu.cn (C.-C. Wang).

https://doi.org/10.1016/j.efmat.2022.05.002
Received 11 April 2022; Received in revised form 8 May 2022; Accepted 17 May 2022

1. Introduction

Adsorption, as an interfacial phenomenon, is widely involved in the separation [1–3], purification [4–6], and catalytic processes [7–9]. Conventional adsorption is generally spontaneous; thus, chemical or energy input is required to achieve desorption. Functional materials that can be structurally switchable by external stimuli such as heat [10,11], redox potential [12,13], pH [14,15], or light [16–22] have aroused wide interests. Among these stimuli, light (particularly concentrated sunlight) has been prioritized because of merits such as by-product-free production, environmental friendliness, and the abundant availability of sunlight [23]. Therefore, light-response adsorption and desorption are exciting strategies for drug delivery, gas separation, and even sample pretreatment [24–29]. MOFs have substantial advantages in the fields of gas, heavy metal, dyes and antibiotics adsorption due to their ultra-high specific surface area (up to Langmuir surface areas of 10400 m^2/g), tunable pore size, and designable functional structures [30,31]. To date, many MOFs with excellent adsorption properties have been developed for ultra-efficient pollutant removal. Our group designed and synthesized a novel, graphene-like 2D-MOF BUC-17, which could adsorb Congo red (CR) with an adsorption capacity of 4923.7 mg/g at 298 K [32]. Our group adopted a post-modification strategy for producing defective NH_2-UiO-66 to boost its adsorption activity toward Pb^{2+}, aided by the construction of hierarchical pores [5]. In addition, we proposed to eliminate and recover noble Ag(I) from simulated silver-plating wastewater, adopting NH_2-MIL-125(Ti) as an effective adsorbent, which could be desorbed to regenerate NH_2-MIL-125 or calcined to produce a Ag/C/TiO_2 photocatalyst [6].

The fabrication strategies of light-responsive adsorption–desorption MOFs and their composites can be divided into four categories: i) MOFs being modified by azobenzene (azo) ligands with excellent light-response performances; ii) MOFs being synthesized from ligands with light-responsive molecular switches; iii) MOF composites being fabricated from pristine MOFs and a secondary component with light-response adsorption/desorption properties; and iv) MOFs containing light-responsive guest molecules in their pores [33,34].

Ligands with light-responsive properties like azo and azo derivatives, as well as photo-responsive molecular switching ligands such as spiropyran and diarylvinyl ligands, were often used to design and synthesize light-responsive MOFs [35,36]. Currently, the light-responsive adsorption and desorption by light-responsive MOFs mainly depend on the *cis–trans* isomerization caused by photoisomerized ligands modified on the inner surface or the surface of MOFs, in which the photoisomerization can adjust the pore size distribution and internal electron configuration of the MOFs [37]. However, reports on the use of photoisomerized ligands as MOF skeletons to regulate the adsorption and desorption of MOFs are rare [38]. Depending on the different strategies for using azo functional groups in MOFs, these light-responsive MOFs can be divided into three generations (Fig. 1) [39]. The first generation mainly uses light-responsive guest molecules to achieve light-response adsorption and desorption. For example, azo dye molecules are loaded in MOF channels [33]. The second generation mainly comprises MOF materials modified with a light-responsive linker side chain in the MOF channel to regulate the internal pore size and electron distribution of MOFs; the third generation mainly includes the skeleton of MOFs designed with light-responsive linker backbones, such as azo ligands and *trans*–1,2-bis(4-pyridyl)ethylene (4,4′-bpe) [40]. With the development of light-responsive MOFs, researchers have not only realized the light-responsive adsorption and desorption of small gas molecules (e.g., CO_2, ethane, and propylene) [41–43] but also extended the light stimulation conditions from the UV region to the visible and near-infrared regions (Table 1) [44,45]. Some researchers even used the magnetic effect of materials to cooperate with light-responsive MOFs and thereby improve their desorption capacities [46]. Other researchers have used light-responsive MOF materials for light-responsive adsorption and desorption of environmental pollutants in water, such as sulfamethoxazole and CR [47,48]. Researchers preferred to extend the excitation wavelength of light-response MOFs to longer regions, mainly because of the renewable and unlimited energy of visible light from the sun [44,45]. In addition, visible and infrared lights are less destructive than UV light, which improves the application prospects of light-responsive MOFs for controlled drug release in the medical industry [44,48,49]. However, to date, the research of light-responsive MOFs in light-responsive adsorption and desorption has mainly focused on light-responsive gas adsorption and desorption processes [41–43]. Meanwhile, the light-responsive

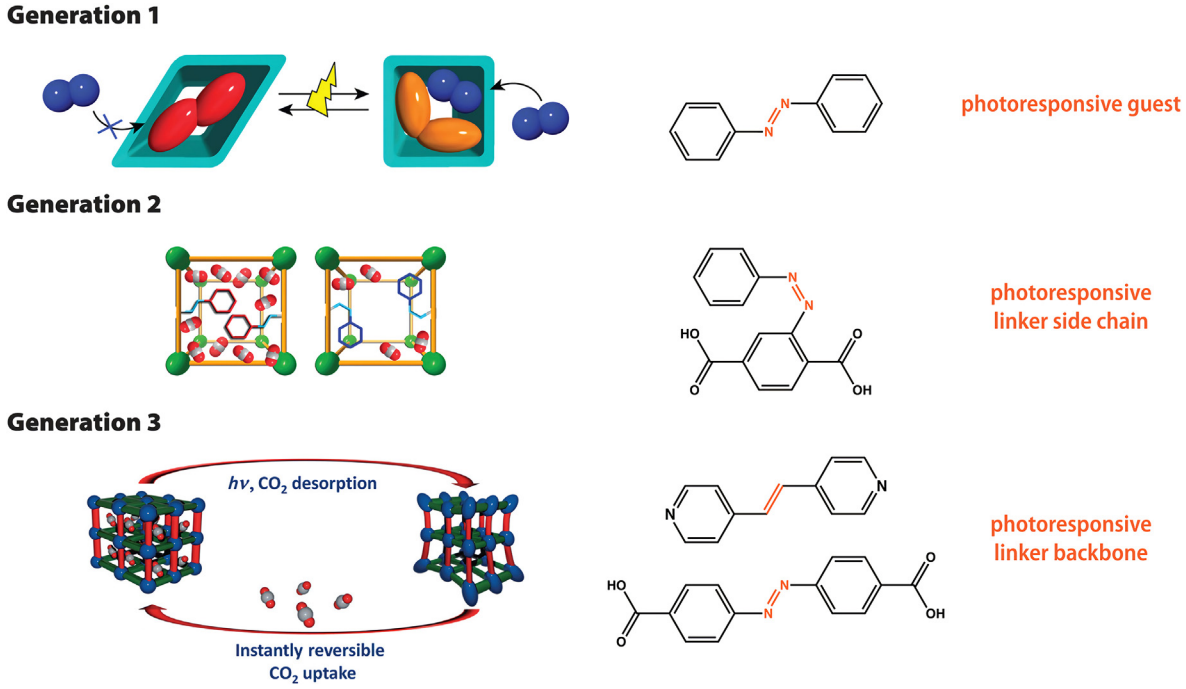

Fig. 1. Three generations of light-responsive MOF materials based on azo functional groups. Reprinted with permission from Ref. [39] (Copyright 2015 American Chemical Society).

Table 1
Recently published light-response MOF materials and their applications.

MOF	Switchable Component	Switching Mechanism	Light	Applications	Reference
PCN-123	2-(phenyldiazenyl)terephthalate	*Cis–trans* isomerization	UV	CO_2 storage and release	[41]
$Cu_2(F_2AzoBDC)_2(dabco)$	(*E*)–2–((2,6–difluorophenyl)diazenyl) terephthalic acid ligand	*Cis–trans* isomerization	Visible	H_2/hydrocarbon separation	[50]
Zn(L)-(bpdc)·solvents	Diarylethene derivative ligand	Ring-opening/closing	UV	CO_2 storage and release	[36]
Azo-IRMOF-74-III	Azo ligand	*Cis–trans* isomerization	UV	Dye (propidium iodide) storage and release	[51]
CAU-5	Dipyridylazobenzene ligand	*Cis–trans* isomerization	UV	Gas storage/release	[52]
PSZ-1	Imidazolate-based Diethienylethene ligand	Ring-opening/closing	UV	Aromatic hydrocarbon filter	[53]
$Cu_2(AzoBPDC)_2(AzoBiPyB)$ SURMOF	2-phenyldiazenyl-4,4′-biphenyldicarboxylic acid and dipyridylazobenzene ligands	*Cis–trans* isomerization	UV	H_2/CO_2 separation	[54]
ECIT-20	4,4′-bpe ligand	[2 + 2] reaction	UV	Allyl alcohol removal, conversion, and release	[55]
$Zn(AzDC)(4,4'\text{-BPE})_{0.5}$	4,4′-bpe and azo ligands	*Cis–trans* isomerization	UV	CO_2 storage/release	[56]
UiO-67	Azo guest	*Cis–trans* isomerization	UV	H_2/CO_2 separation	[57]
Azo-UiO-66	2-phenyldiazenyl terephthalic acid	*Cis–trans* isomerization	UV	N_2/CO_2 separation	[58]
PCN-250	3,3′,5,5′-azo tetracarboxylic acid	*Cis–trans* isomerization	UV	CO_2 storage/release	[38]
mPCN	3,3′,5,5′-azo tetracarboxylic acid	*Cis–trans* isomerization	UV	CO_2 storage/release	[46]
UiO-68-Azo	2′-ptolyldiazenyl-1,1:4,4-terphenyl-4,4-dicarboxylic acid	*Cis–trans* isomerization and the interaction with β-CD	UV	RhB	[48]
$[Zn_2(terephthalate)_2(triethylenediamine)]_n$	Azo guest	*Cis–trans* isomerization	UV	CO_2 storage/release	[33]
UiO-66	5-fluorouracil	N.A.	Near-infrared	5-fluorouracil storage/release	[49]
UiO-66-NH_2/Ag_3PO_4 composites	Ag_3PO_4	Redox	Visible	Sulfamethoxazole storage/release	[47]
UiO-66-NH_2/Ag_2CO_3	Ag_2CO_3	Redox	Visible	Sulfamethoxazole, sulfisoxazole, and sulfamethazine storage/release	[44]
$Co_2L_2(AzoD)_2$·2DMF	3,3′-azodibenzoic acid	*Cis–trans* isomerization	UV	CO_2, CH_4, O_2, CO, and N_2 separation	[59]
GO@MIL-101	Integration of MIL-101 with graphene oxide nanosheets	Light-induced localized heat	UV–vis or UV-vis-near-infrared	ethyl acetate adsorption and release	[45]
Ag/UiO-66	Ag nanocrystals	Light-induced localized heat	Visible	CO_2 storage/release	[60]
UiO-67 Membrane	Azo guest	*Cis–trans* isomerization	UV	CO_2 storage/release	[61]
T/Zr-PDI	*N*,*N*′-di-(4-benzoic acid)-1,2,6,7-tetrachloroperylene-3,4,9,10-tetracarboxylic acid diimide and perylenediimide	Nonradiative relaxation process	Near-infrared	Ethane storage/release	[42]
HKUST-1	Azo and o-tetrafluoroazobenzene guest	*Cis–trans* isomerization	UV and visible	butanediol storage/release	[62]
Mg-IRMOF-74-III	Azopyridine	*Cis–trans* isomerization	UV	CO_2 and N_2 separation	[63]
Ag@ZIF-8	Ag nanocubes	Light-triggered heating	Visible	Propylene storage/release	[43]
UiO-66-NH_2	4-(5-Methoxy-1,2-dimethyl-1H-indol-3-yl)-3-(2,5-dimethylthiophen-3-yl)-4-furan-2,5-dione	Ring-opening/closing	UV	H_2 adsorption/desorption	[64]
Coumarin-modified Zn-MOF-74	Coumarin	Photodimerization	UV	U^{VI} ion storage/release	[65]

MOF materials in water have rarely been studied, which substantially limits their practical application potentials. However, light-responsive adsorption and desorption in an aqueous environment have important practical significances and values for sewage treatment and medical delivery, such as enrichment and regeneration of pollutants in sewage or controlled release of drugs in organisms [48]. Therefore, the adsorption and desorption processes of light-responsive MOF materials in an aqueous environment will be an important research content for light-responsive MOFs. The development for MOF materials with good water stability, stable molecule structures, and excellent light-responsive adsorption–desorption capabilities in the visible or near-infrared light region might be appreciated.

In recent years, light-responsive MOF adsorbents have attracted increasing attentions from researchers, as the adsorption/desorption process can be controlled by light [34,57]. This article presents a brief review of the current design strategies for MOFs with light-induced desorption. In particular, discussion and comments are provided for MOFs with high water stability, aiming to accomplish the light-response release of target substances in an aqueous environment.

2. MOFs containing azo groups

Azo (–N═N–), as a popular light-responsive organic functional group, can achieve efficient reversible photoisomerization because the azo bond can transform between *cis* and *trans* modes upon irradiation with different wavelengths of light (*trans*: $\lambda_{max} \approx 370$ nm; *cis*: $\lambda_{max} \approx 460$ nm) [66–68]. This isomerization leads to a distance alteration between the para-carbon atoms in an azo molecule from 0.9 nm in the *trans* isomer to 0.55 nm in the *cis* one [69]. Recently, three popular strategies have been proposed to introduce azo into the structure of MOFs [37,70,71]: (i) the azo is modified on the linker as a side branch [41,72]; (ii) the azo ligand is directly used as the linker in the as-prepared MOFs [38,73]; and (iii) the azo guest molecule is introduced into the structure of MOFs during synthesis or post-synthesis [62,70,74]. Adopting azo ligands as a connector in MOF skeletons for optical absorption stripping is challenging because a lack of free space or the destruction of the lattice may occur during the *cis–trans* isomerization of azo [70].

Modifying an azo group to the side chains of the linkers to adjust the pore structure of light-responsive MOFs is one of the most popular methods

for light-responsive adsorption and desorption [41,72]. Zhou and co-workers [75] solvothermally synthesized the rigid MOF PCN-123 (PCN represents porous coordination networks) using 2-(phenyldiazenyl) terephthalate and $Zn(NO_3)_2{\cdot}6H_2O$ as precursors. In a typical reaction, the azo functional groups in the 2-(phenyldiazenyl) terephthalate are mainly *trans* isomerized (Fig. 2a), in which the UV–visible absorption peaks at 320 nm and 430 nm can be ascribed to π-π* and n-π*, respectively (Fig. 2b and c). Under UV (302 or 365 nm) irradiation, absorption peaks at 320 nm and 430 nm gradually decreased and increased, respectively, indicating that UV-photoinduced *cis–trans* isomerization occurred (Fig. 2a). The cubic cavities in PCN-123 are occupied by many azo functional groups, resulting in photoinduced structural rearrangement in the process of photo-stimulation of azo *cis–trans* isomerization. This photoinduced structural rearrangement also enables the potential for photoinduced gas adsorption and desorption. The absorption capabilities of PCN-123 toward CO_2 decreased from 22.9 cm^3/g (1 bar) to 16.8 cm^3/g (1 bar) before and after exposure to UV light for 60 min (a 26.6% decrease). Interestingly, when the adsorption capacity was retested at the same temperature, the overall adsorption capacity of PCN-123 to CO_2 decreased by 53.9% compared to the initial PCN-123 (Fig. 2d). The alternation of adsorption capacity under UV irradiation contributed to the steric hindrance of azo functional groups near the cubic cavities in PCN-123.

Compared with fresh PCN-123, the CO_2 adsorption capacity of heat-treated PCN-123 wrapped in aluminum foil under 60 °C for 20 h increased by 13.3% (Fig. 2d). However, the complete *trans*–PCN-123 (synthesized in the dark) did not show the same CO_2 uptake increase when heated and regenerated, indicating that the removal of residual organic small molecules in the pores by heating did not cause the increase in CO_2 adsorption ability. Hence, the *cis–trans* isomerization of azo functional groups in the pores of PCN-123 resulted in the change in CO_2 adsorption capacity. The powder X-ray diffraction (PXRD) peak positions of the *trans* isomer of PCN-123 (before UV irradiation) and the *cis* isomer (after UV irradiation) were identical; however, the peak intensities were obviously different. The structure envelopes from the PXRD data revealed that the electron density of the *cis* isomer near the Zn_4O cluster was higher than that of the *trans* isomer, implying that gaseous CO_2 accessed and occupied the space of the cluster with difficulty [76,77]. Furthermore, the pore size distribution reached a peak at 1.0 nm and 1.1 nm before and after UV irradiation, respectively (Fig. 2e). The pore size distribution curves of the pristine PCN-123 sample and the regenerated one via heat treatment were identical, demonstrating that the variation in pore size distribution is caused by the isomerization of organic ligands. PCN-123 could be adopted as a smart adsorbent for photoinduced CO_2 desorption, which might facilitate developing a facile routine of sorbent regeneration or stimuli-response drug delivery [41].

Ladewig et al. [58] prepared different azo-UiO-66 MOFs from 2-phenyldiazenyl terephthalic acid (L_1) and terephthalic acid (L_2) in different proportions (25:75, 50:50, and 75:25). In this work, azo functional groups were introduced into the pores of UiO-66 by substituting the organic ligand linkers, which provided a new idea for the application of light-responsive MOFs for light-response adsorption and desorption. The light-responsive azo ligand linker in azo-UiO-66 affected the CO_2 adsorption and CO_2/N_2 selectivity. As shown in Fig. 3a and b, all the synthesized azo-UiO-66 MOFs possessed a crystalline structure similar to UiO-66. The mixed-linker in azo-UiO-66 was confirmed by ^1H nuclear magnetic resonance (^1H NMR), UV–vis, and attenuated total reflectance Fourier-transform infrared (ATR-FTIR) spectroscopy. The ligand ratio calculated based on NMR spectral data was different from that under synthetic conditions, which might have contributed to L_1 having a larger structure than L_2 during the coordination process. The steric hindrance led to L_1 having more difficulties than L_2 in interacting with the metal clusters. The pore volume and BET surface area decreased with an

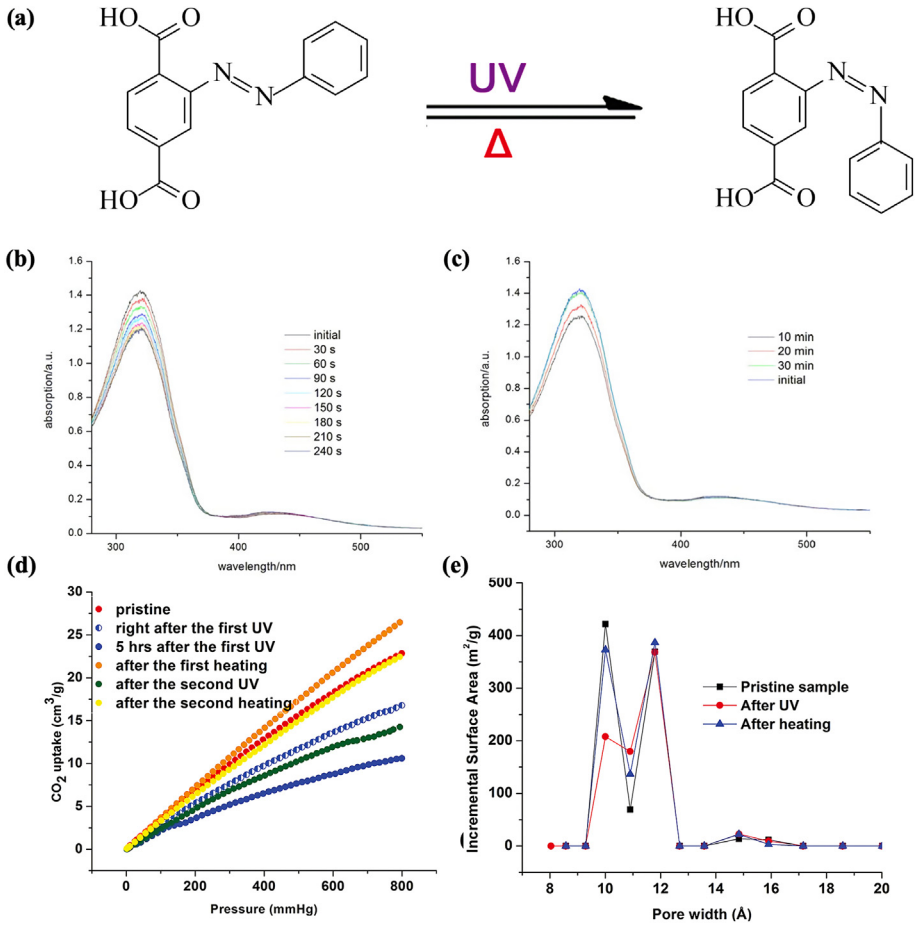

Fig. 2. (a) *Trans*-to-*cis* isomerization of 2-(phenyldiazenyl)terephthalate in PCN-123 resulting from UV irradiation and heat treatment; (b) UV–vis absorption spectrum of PCN-123 every 30 s during exposure to UV light (365 nm); (c) UV–vis absorption spectrum of PCN-123 after every 10 min heating at 60 °C; (d) CO_2 sorption isotherms of PCN-123 under various conditions (triggered by UV irradiation or heating); (e) the pore size distribution of PCN-123 before and after UV irradiation and heating. Reprinted with permission from Ref. [75] (Copyright 2011 American Chemical Society).

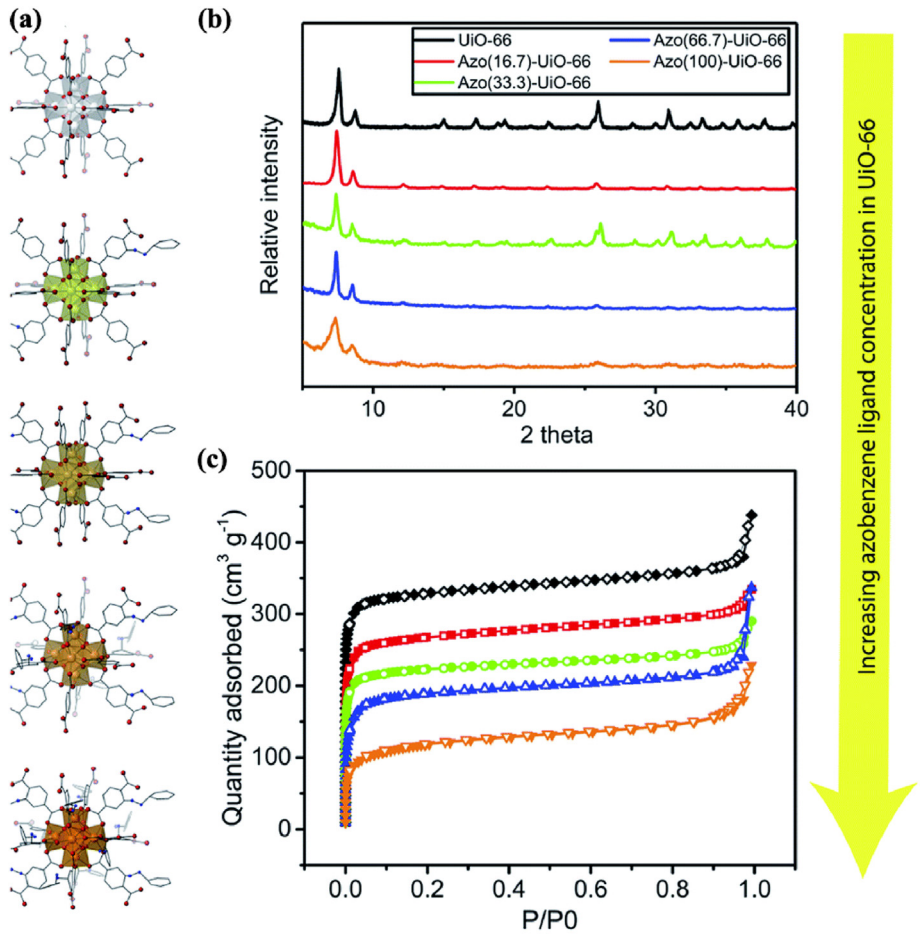

Fig. 3. (a) Hypothetical structural units of UiO-66 with different proportions of mixed ligands; (b) the PXRD patterns; and (c) N_2 adsorption and desorption isotherms of UiO-66 and azo(X)-UiO-66. Reprinted with permission from Ref. [58] (Copyright 2019 Royal Society of Chemistry).

increasing number of azo ligands (Fig. 3c) because the azo with a larger molecular size could occupy the pore in the framework. The pore size of azo (66.7)-UiO-66 and azo (100)-UiO-66 (about 0.9 nm) is larger than that of UiO-66 (about 0.7 nm), probably as a result of the framework stretching to accommodate more azo. However, the addition of an azo ligand in a certain range (0–33.3%) has no obvious effect on CO_2 adsorption capacity compared with UiO-66.

Despite many studies on the use of azo-modified MOFs to achieve light-response adsorption, desorption, and separation of gas targets in the environment, few studies are available on using azo photoisomerization to achieve light-controlled release of targets in an aqueous environment. If light-responsive adsorption and desorption can be performed in an aqueous environment, it will not only greatly expand the scope of the research field but also enhance its potential value in future practical applications, such as pollutant removal in wastewater, light-response drug delivery, and resource recycling. Yaghi et al. [51] synthesized an azo functionalized isoreticular azo-IRMOF-74-III [$Mg_2(C_{26}H_{16}O_6N_2)$] and used it in light-response absorption and desorption of the luminescent dye propidium iodide in water. Under different light stimulations, azo ligands of azo-IRMOF-74-III underwent *cis–trans* isomerization, leading to a substantial change in the molecular length and, therefore, the one-dimensional pore size of azo-IRMOF-74-III (Fig. 4a). After the propidium iodide dye was introduced into azo-IRMOF-74-III, no desorption of the luminescent dye was detected under ambient conditions (Fig. 4b–d). However, triggered by 408-nm light, the dye was released from the holes in the azo-IRMOF-74-III because of the rapid oscillations caused by the repeated isomerization of azo functional groups. The size of this dye molecule free of counterions was $8 \times 11 \times 16$ Å, which matches well with the pore size of azo-IRMOF-74-III (0.83–1.03 nm). This photoinduced cargo release process was achieved by adjusting the conformation of azo driven by an appropriate wavelength of light. This report indicated that azo-MOF could store dye molecules and release them through a photoisomerization process in an aqueous system.

The design of stimulus-response MOFs with high water stability of photo-responsive release in the liquid phase is essential for light-response drug delivery. Meng et al. [48] synthesized a novel azo-MOF (UiO-68-azo) with good water stability and light-response ability. UiO-68-azo can act as a platform to construct interactions between the β-cyclodextrin (β-CD) and its surficial azo side chain (Fig. 5a). The obtained UiO-68-azo-MOF can perform light-response release of the loaded drug under UV light and can achieve sustained release by adding guest rival molecules. UiO-68 was synthesized with 2′-ptolyldiazenyl-1,1:4,4-terphenyl-4,4-dicarboxylic acid and then loaded with the cargo rhodamine B (RhB), which was then sealed with β-CD as a gate. Because the affinity of β-CD and *trans*–azo is considerably higher than that of *cis*–azo in water, it can induce the azo groups in the side chain of the ligand to undergo *cis* isomerization by UV light, which in turn makes the closed door open to release the RhB. Interestingly, this desorption process can be triggered by introducing competing binding agents, such as amantadine. The experimental results showed that the release of RhB could be further achieved by using adhesive to desorb a part of the drug and then turning on the light, which provided more options for drug release in complex environments (Fig. 5b).

The third generation of light-responsive MOFs is synthesized by using light-responsive ligands directly as the “backbone” of the MOFs and is considered the most promising and challenging light-responsive MOF materials [39]. Compared with the first two generations of

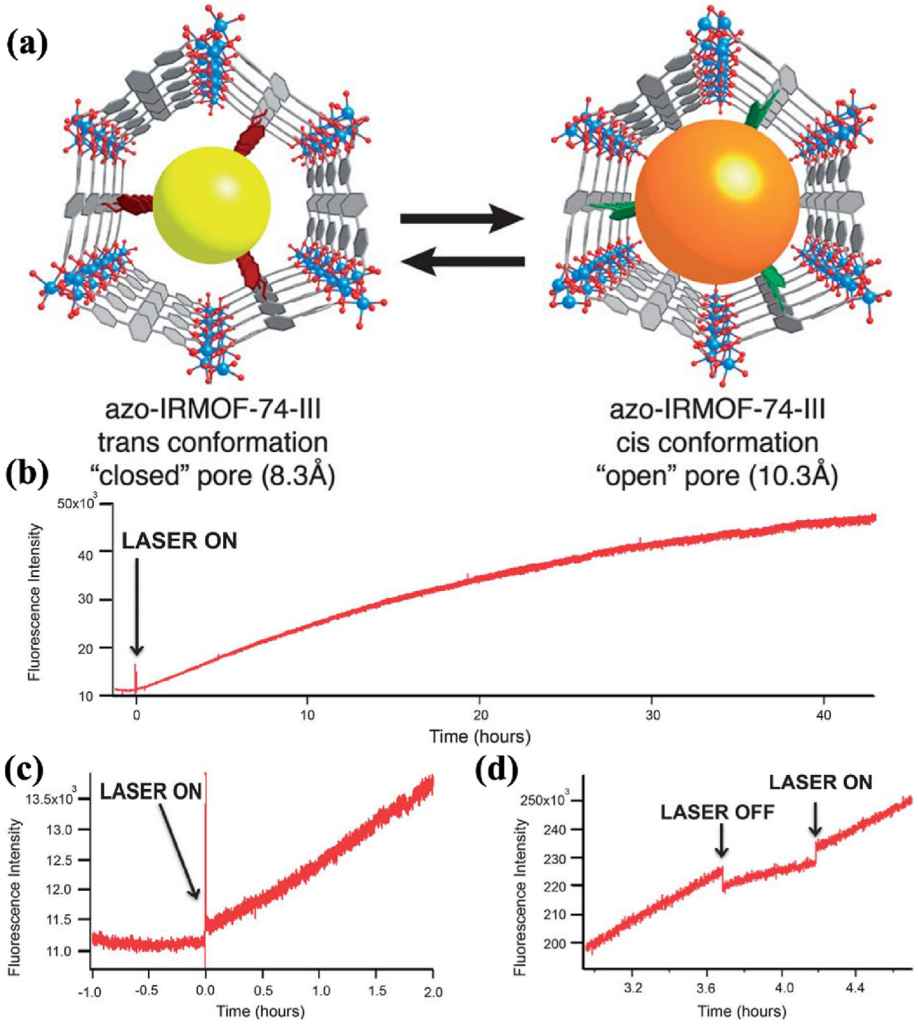

Fig. 4. (a) Ideal azo-IRMOF-74-III one-dimensional pores under *cis* and *trans* conditions and the variation in the pore size induced by azo functional groups in the pores under *trans* and *cis* isomerization; (b) desorption of propidium dye from MOF-74 under laser irradiation; (c) the baseline and start of laser irradiation; (d) an on/off trial. Reprinted with permission from Ref. [51] (Copyright 2010 Royal Society of Chemistry).

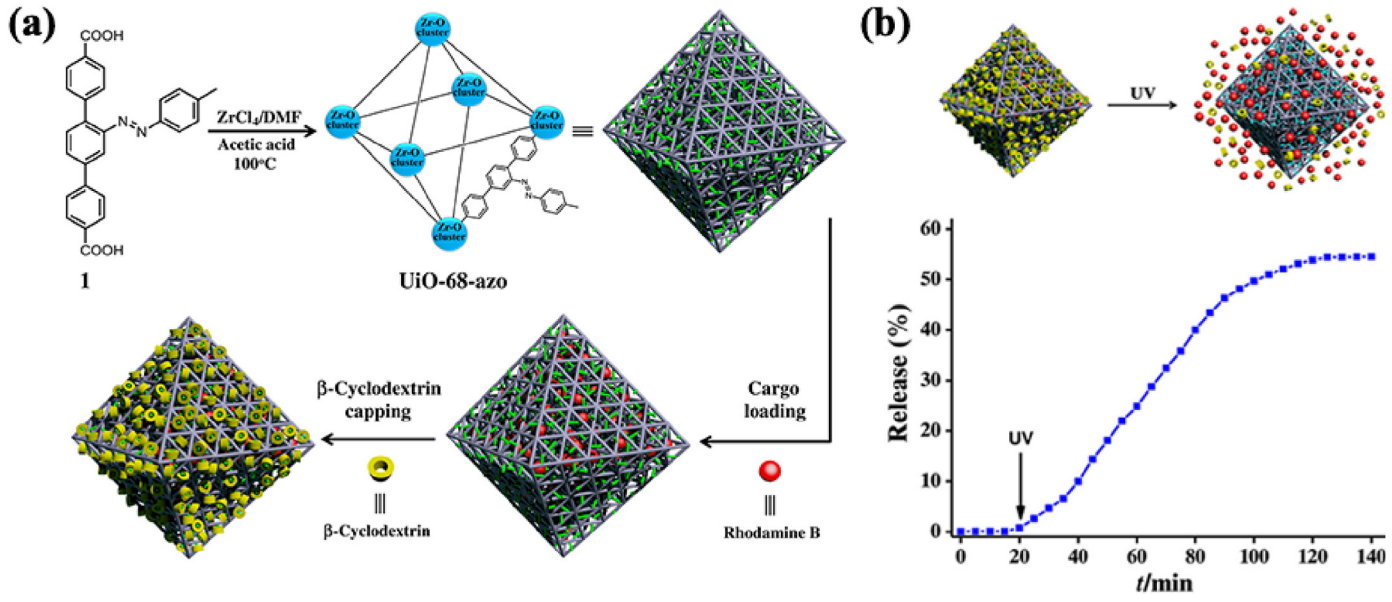

Fig. 5. (a) Schematic diagram of the synthesis process of UiO-68-azo, and further, RhB was encapsulated in the structure of UiO-68-azo, and then β-CD was coated on the surface; (b) RhB is released step-by-step by adding amantadine and then UV irradiation. Reprinted with permission from Ref. [48] (Copyright 2021 American Association for the Advancement of Science).

light-responsive MOF materials, the third generation can most directly affect the skeleton itself, thus allowing the maximum and most direct photoinduced isomerization of materials [39]. Considering that the pillar ligand *trans*–1,2-bis(4-pyridyl)ethylene (4,4′-bpe) in a metal complex can demonstrate *cis–trans* photoisomerism [78–80], 4,4′-bpe along with azo-4,4′-dicarboxylytic acid (AzDC) were introduced to bond with Zn^{2+} to form the interpenetrated Zn(AzDC)(4,4′-bpe)$_{0.5}$ [40]. Compared with the previous light-responsive azo-MOFs, the *cis–trans* isomerized azo-groups in Zn(AzDC)(4,4′-bpe)$_{0.5}$ are like the skeleton of MOFs (the third generation of light-responsive MOFs) rather than the modified groups in the pores of the MOFs [81]. The light-responsive investigation results revealed that AzDC and 4,4-bpe ligands in Zn(AzDC)(4,4′-bpe)$_{0.5}$ can be converted into *cis* isomerism under UV light (200–500 nm) excitation, in which they can revert to the *trans*–state when UV stimulation is stopped. The *trans* and *cis* isomerism of AzDC can be detected from excitation spectra at 455 and 390 nm, which were attributed to the n-π* and π-π* transitions, respectively (Fig. 6a). Notably, the *trans* isomer of 4,4-bpe in Zn(AzDC)(4,4′-bpe)$_{0.5}$ demonstrated the overlapping excitation bands of (metal-to-ligand charge transfer (MLCT) and ligand-to ligand charge transfer (LLCT) in the region of 310–375 nm, resulting in its *trans–cis* isomerization upon irradiation in this region (Fig. 6b). Interestingly, the free 4,4-bpe ligand did not display photoactivity in the solid state. Zn(AzDC)(4,4′-bpe)$_{0.5}$ exhibited an open topology with a strong adsorption capability toward hydrogen and CO_2 (Fig. 6c) [82].

Zn(AzDC)(4,4′-bpe)$_{0.5}$ performed an excellent dynamic switching (unfiltered light in the wavelength range of 200–500 nm and continuous switching on at an approximately 10 min interval) in CO_2 uptake (Fig. 6c). The CO_2 desorption capacity of Zn(AzDC)(4,4′-bpe)$_{0.5}$ under static and dynamic light irradiation are 42% and 64%, respectively, as the light irradiation increased the Zn(AzDC)(4,4′-bpe)$_{0.5}$ surface energy to decrease the interactions between CO_2 and the MOF surface for triggering the CO_2 desorption. A series of control experiments further confirmed that the dynamic light response of the MOF was not caused by artificial or minor localized heating of the material in the experiment.

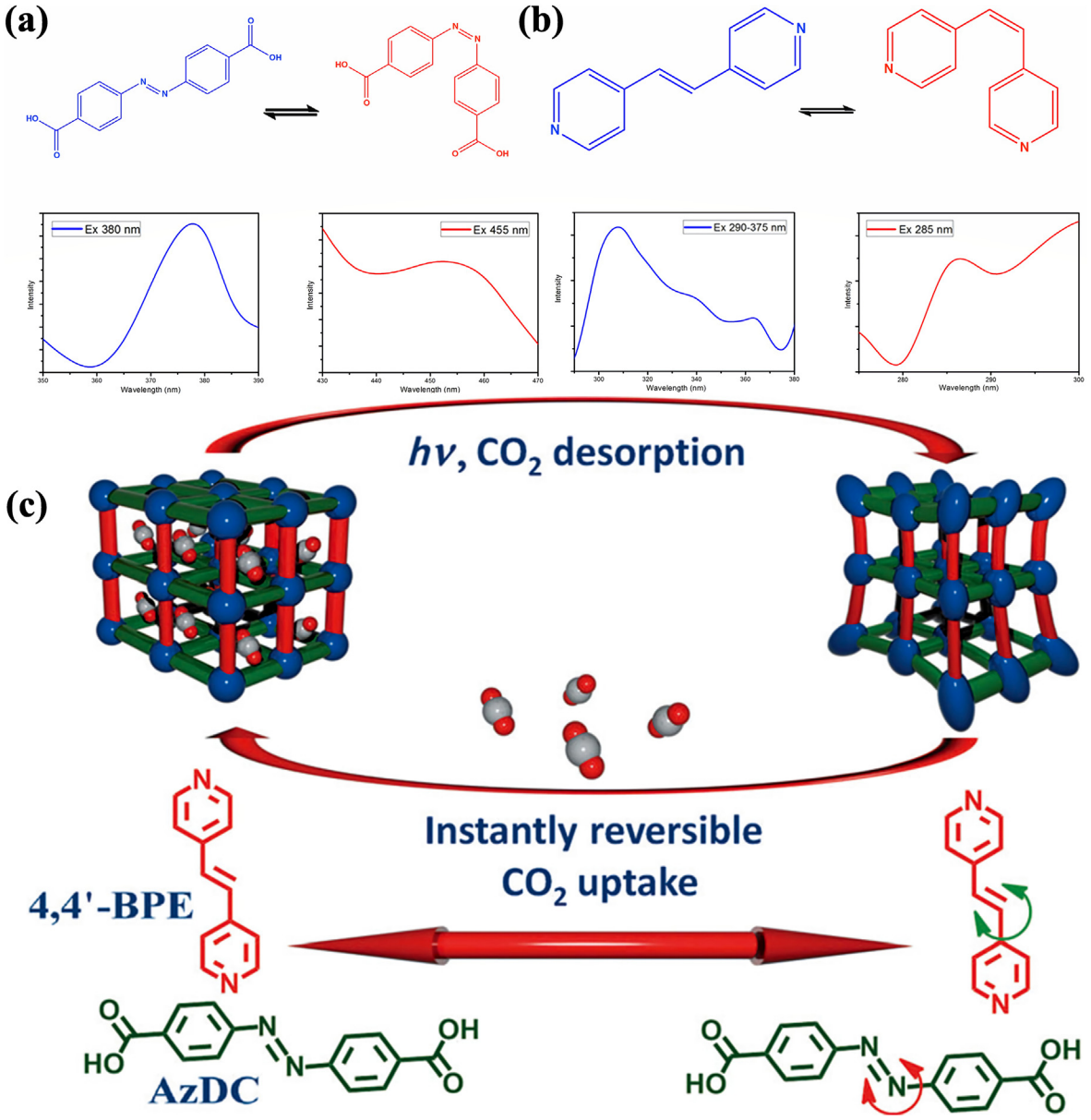

Fig. 6. (a) Excitation spectra of the AzDC linker in Zn(AzDC)(4,4′-bpe)$_{0.5}$ and the individual AzDC linker at emission wavelengths of 370 nm (red) and 460 nm (blue); (b) the excitation spectra of 4,4′-bpe ligand in Zn(AzDC)(4,4′-bpe)$_{0.5}$ at emission wavelengths of 250 nm (blue) and 370 nm (blue); (c) reversible adsorption toward CO_2 of the light-responsive MOF Zn(AzDC)(4,4′-bpe)$_{0.5}$ under dynamic photo-switching. Reprinted with permission from Ref. [40] (Copyright 2013 WILEY-VCH).

The Fourier-transform infrared (FTIR) spectrum showed that the peak intensities at 550 cm^{-1} (C–C–C and C–C–N bonds) and 537 cm^{-1} (C–C–N bonds) increased noticeably after light irradiation, indicating the change in the bending mode of the corresponding functional groups of AzDC ligands [83]. These changes may lead to an increase in the surface energy of the MOF and, in turn, cause the release of adsorbed CO_2. The 1516 cm^{-1} peak (N═N bonds) of the free AzDC ligands changed after a slight change in light irradiation, indicating that the stretching mode of the *cis*–N═N structure has higher bond energy [84]. This transformation was not observed in the framework, suggesting that AzDC was restricted in the structure, which was further confirmed by no change in XRD of $Zn(AzDC)(4,4'\text{-bpe})_{0.5}$ before and after light illumination. In addition, *trans*–AzDC and *cis*–AzDC linkers in the structure of the framework were found to oscillate periodically between the two isomers in a complementary manner under continuous irradiation of 365 nm or 460 nm. CO_2 could be desorbed upon irradiation by either light source (365-nm filtered and unfiltered light with the wavelength range of 200–500 nm), in which the filtered light of 365 nm is more efficient than unfiltered light. This effect is more substantial under high partial pressures. Unfiltered light in the combustion recovery stream also obtained a very comparable response. This study is the first case to establish an experimental protocol for low-energy CO_2 adsorption and desorption using the

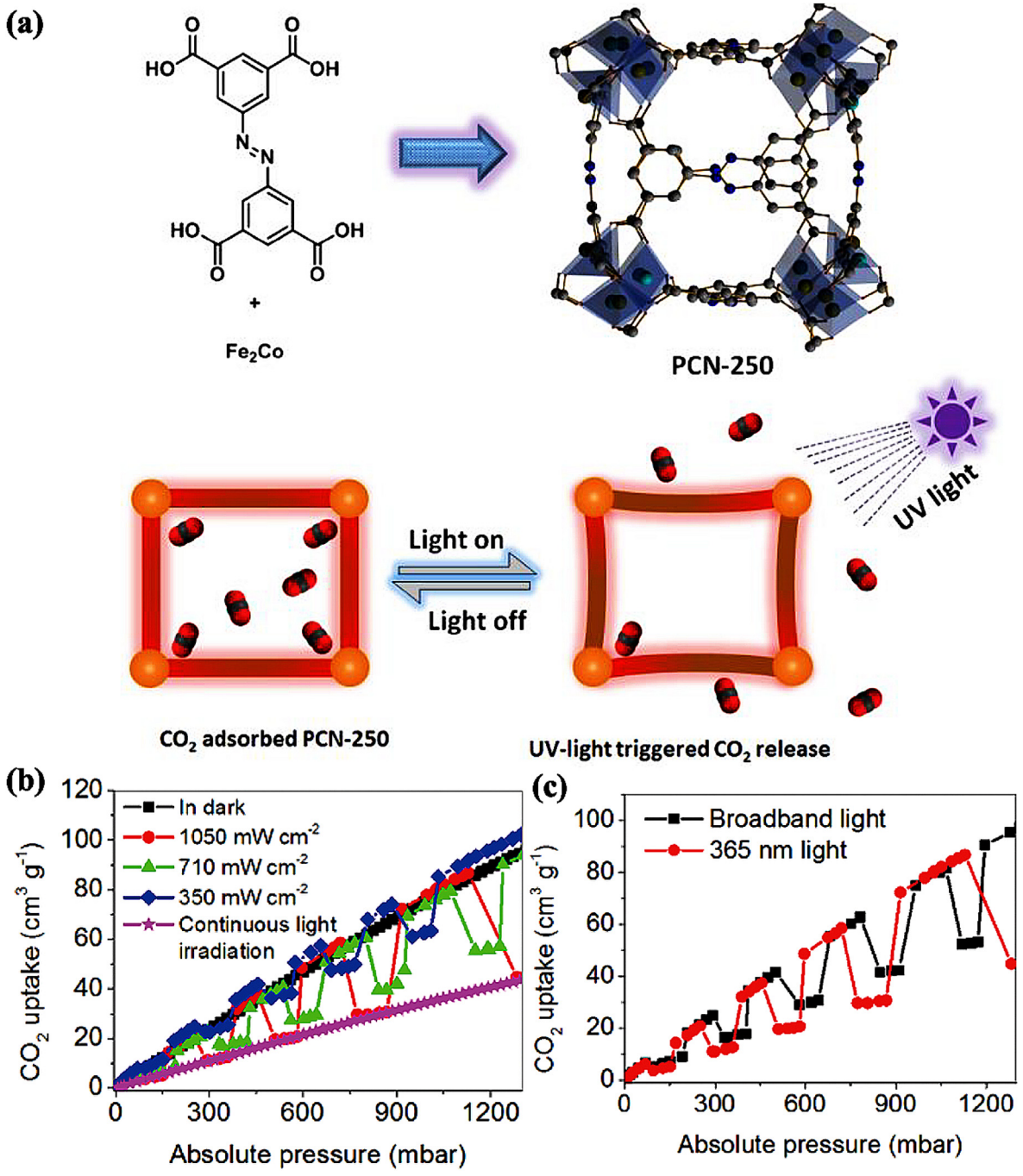

Fig. 7. (a) Crystal structure of PCN-250 and the absorption and desorption diagram of CO_2 in PCN-250 under UV light through reversibly suppressed bending of the ABTC ligand; (b) the light-response adsorption and desorption isotherms of CO_2 by PCN-250 were illuminated intermittently under different intensities of 365-nm light, without light, and with continuous irradiation of 365-nm light at 298 K; (d) photoinduced CO_2 adsorption and desorption isotherms of PCN-250 under unfiltered light (1050 mW/cm^2) and 365-nm light at 298 K. Reprinted with permission from Ref. [38] (Copyright 2016 WILEY-VCH).

light-responsive adsorption–desorption property of an MOF.

The construction of the reported light-response MOFs for gas release mainly depended on weak electrostatic interactions between metal ions and carboxylate linkers, which demonstrated structural instability [38,85,86]. It is challenging and desired to construct photo-responsive MOFs with good water stability and chemical resistance for light-response desorption of gas in a natural environment. Hill et al. [38] reported a light-responsive PCN-250 with a robust structure using a 3,3′,5,5′-azo tetracarboxylic acid ligand and $Fe_2Co(\mu_3\text{-}O)(CH_3COO)_6$ metal clusters (Fig. 7a). PCN-250 was structurally stable in aqueous solution and organic solvents. Similar to the results of previous reports, PCN-250 maintained its structural integrity in water for more than six months [85]. This stable structure is mainly attributed to the $Fe_2Co(\mu_3\text{-}O)(CH_3COO)_6$ metal clusters providing hard Lewis acid sites for carboxylic acid ligands. ABTC ligand, as a derivative of azo, presented *cis–trans* isomerism under UV light. Hence, the structure of PCN-250 can present nonperiodic bending under UV light to realize light-triggered CO_2 desorption.

As shown in Fig. 7b, PCN-250 displayed light flux-dependent desorption capacities for CO_2 with 365-nm light. The desorption capacities of PCN-250 under 710 mW/cm^2 and 350 mW/cm^2 at 580 mbar are 36.2% and 23.2%, respectively, which are 62.9% and 40.3% of that under 1050 mW/cm^2, respectively. In addition, under the same optical power (1050 mW/cm^2) and atmospheric pressure (580 bar), the CO_2 desorption capacity (57.5%) of the 365-nm light source is better than that of the broadband light source (36.4%), further indicating that the higher light flux led to a stronger CO_2 desorption capacity of PCN-250 (Fig. 7c and d). The BET data showed that the photoinduced gas desorption process took less than 5 min for each switching cycle. The CO_2 release induced by 365-nm UV light and unfiltered

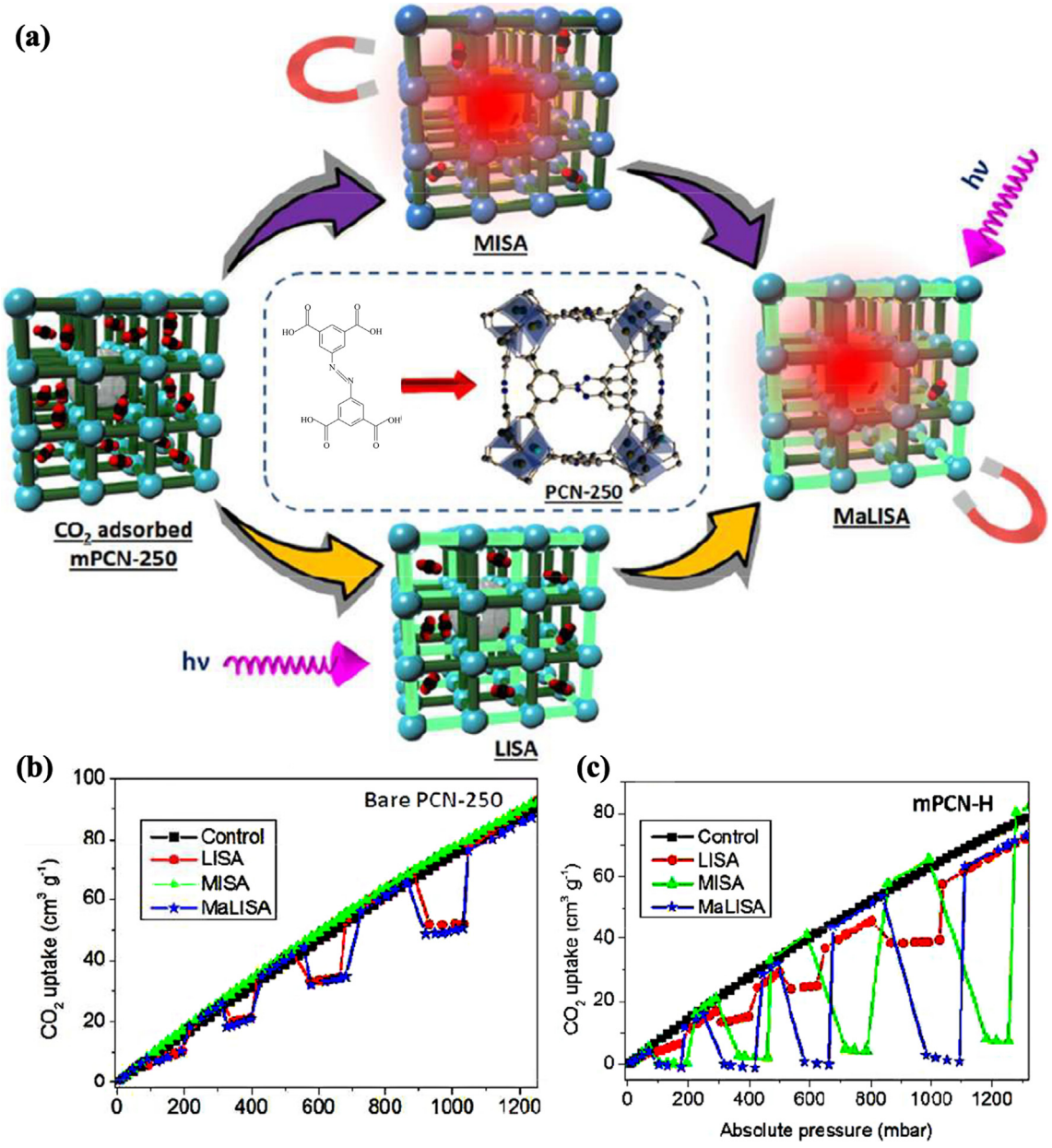

Fig. 8. (a) Schematic diagram of CO_2 desorption under dual stimulation of UV light and a magnetic field in a MaLISA process; (b) the switching cycles of CO_2 uptake and release in bare PCN-250; (c) CO_2 adsorption and desorption by LISA, MISA, and MaLISA processes, in which all dynamic CO_2 adsorption profiles were achieved by intermittently exposing the sample to 365-nm UV light (LISA process) and/or an alternating magnetic field (17.6 mT, MISA process) at 298 K. Reprinted with permission from Ref. [46] (Copyright 2016 The Royal Society of Chemistry).

light increased the sample temperature by ~2.1 °C and ~5.5 °C, respectively (1050 mW/cm^2, 5 min). The desorption capacity of PCN-250 toward CO_2 at 298 K was only 2.2% lower than that at 300 K, indicating that UV light was the main cause of CO_2 desorption from PCN-250.

For highly efficient light utilization, light-responsive desorption, and regeneration of MOF materials, sufficient space is desired for light transmission to MOFs for large-scale engineering applications. Therefore, a single stimulus response may result in reduced use of infrastructure volume. Introducing double or multiple stimuli to fine-tune the stimulus release behavior of substances is also an effective method and has attracted the attention of researchers in recent years [87]. Light induction swing adsorption (LISA) and magnetic induction swing adsorption (MISA) are the adsorption and desorption processes controlled by alternating light and alternating magnetic fields, respectively [60,88]. LISA is also known as the light-response adsorption and desorption alternating process. MISA is a strategy for inducing MOF adsorption and desorption using alternating magnetic fields. The MISA process involves the introduction of magnetic nanoparticles into the MOFs as a local nanoheater for local heating and desorption [46]. The combination of the LISA and MISA processes (MaLISA) can effectively improve the desorption ability of materials and the adaptability of materials to specific environments in practical application [46]. Li and coworkers [46] reported a dual-stimulus-response MOF magnetic PCN-250 (mPCN), which exhibited a dual response to UV light and magnetism (Fig. 8a). mPCN was obtained by integrating magnetic nanoparticles (Fe_3O_4 NPs) with MOFs. Magnetic nanoparticles exposed to alternating magnetic fields acted as nanoheaters to generate local heat. In mPCN, UV light and magnetism synergically achieved a high desorption efficiency (96.8% CO_2, 1 bar) through a MaLISA process, which ensured a low-energy and effective strategy for regenerating large-scale MOF adsorbents. Magnetic fields could penetrate the MOFs to regenerate the adsorption dose on a large scale.

The researchers also introduced different mass percentages of magnetic Fe_3O_4 NPs to produce magnetic PCN-250, named mPCN-L (1.3 wt %), mPCN-M (2.4 wt%), and mPCN-H (7.3 wt%). The local temperature of mPCN-H increased by 97.0 °C after being exposed to a magnetic field (17.6 mT at 279 kHz) for 8.0 min, which was higher than those of mPCN-L (17.4 °C), mPCN-M (32.5 °C) and PCN-250 (0 °C). In addition, mPCN and the pristine PCN-250 only increased 3.1–3.6 °C under 365-nm UV light (1.05 W/cm^2). The BET surface area of mpCN-H was 18.9% lower than that of pristine PCN-250 because of the introduction of more nonporous MNPs into the MOF matrix [85,88]. The CO_2 adsorption capacity of PCN-250 and MPCN-H at 298 K (1 bar) are 75.6 and 61.9 cm^3/g, respectively, because their specific surface areas differ (Fig. 8b and c). mPCN-M performed different CO_2 desorption effects under different stimuli with 30% (90 mbar, 5 min) desorption efficiency of adsorbed CO_2 under UV irradiation and 62.2% (178 mbar, 2 min) desorption efficiency of adsorbed CO_2 under an alternating magnetic field. Interestingly, mPCN-M being first exposed to UV light and then switched to the alternating magnetic field increased the CO_2 desorption efficiency to 62.2% in 2 min. However, as the magnetic field was shut off and then the UV lamp was turned on, the desorption efficiency of CO_2 decreased to 31.9% in 5

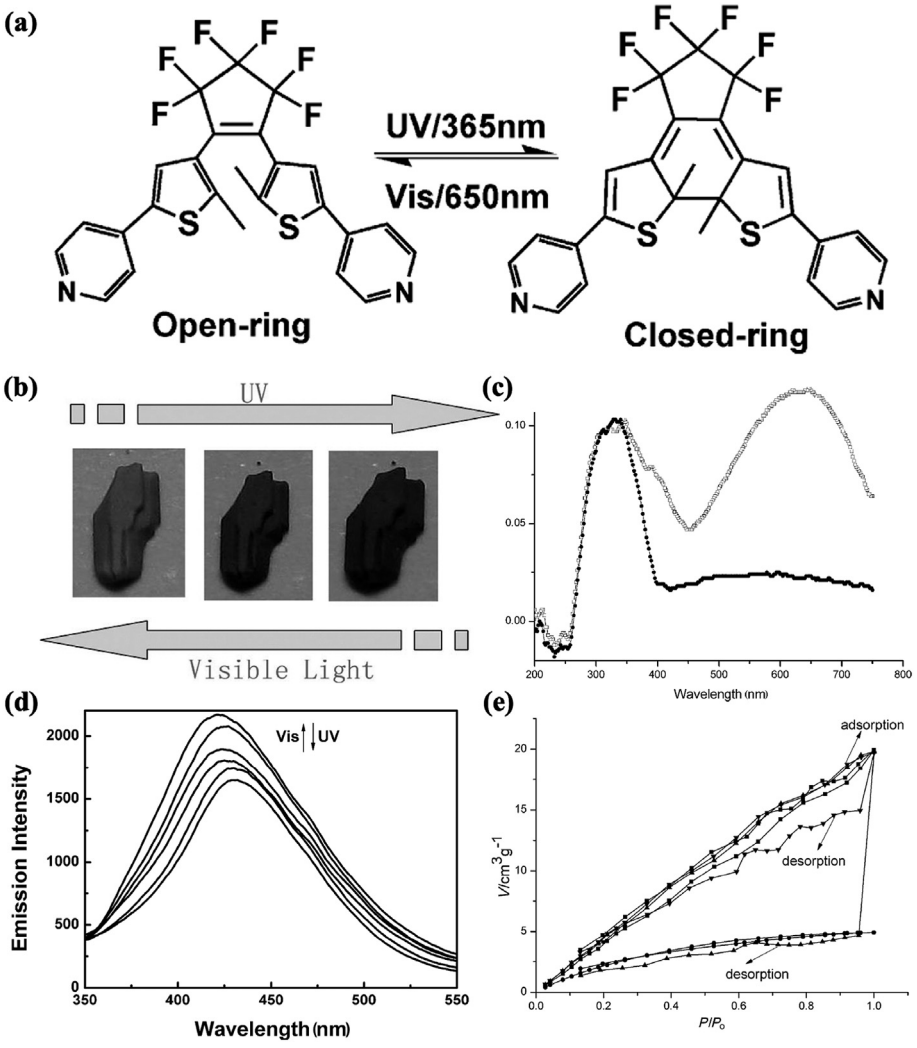

Fig. 9. (a) Structure and photochemical transformation of the diarylethene derivative (L) upon UV and visible light irradiation; (b) photochromic reaction of single-crystal Zn(L)-(bpdc)·solvents exposed to UV and visible light; (c) absorption spectra of solid Zn(L)-(bpdc)·solvents under UV irradiation for 1 min and unirradiated, respectively (□: under UV light for 1 min, •: pristine sample); (d) luminescence spectrum of solid Zn(L)-(bpdc)·solvents under UV light and visible light (the spectra were recorded under UV or visible light irradiation every 5 s); (e) the static and dynamic CO_2 isotherms of Zn(L)-(bpdc)·solvents under different external stimuli (■: under UV light, ●: under ambient conditions ▲: adsorption under UV light, desorption under visible light, ▼: adsorption under UV light, desorption under ambient CO_2, 298 K). Reprinted with permission from Ref. [36] (Copyright 2014 WILEY-VCH).

min, and the adsorption capacity of CO_2 returned to its original state after the UV light was turned off. Evidently, the dual stimulation of the magnetic field and UV light accelerated the desorption of CO_2 and increased the CO_2 desorption capability. Under the dual action of UV light and a magnetic field, mPCN-H significantly increased the CO_2 desorption capacity up to 96.8%, which further illustrated the promoting effect of dual stimulation on CO_2 desorption (Fig. 8c). Compared with mPCN-H, PCN-250 only responded to UV stimulation (Fig. 8b and c). Regarding the adsorption isotherms of CO_2 and the individual magnetic field stimulated desorption process, the minimum regenerative energy requirements of MPCN-H were 2.01 MJ/kg CO_2, comparable to the energy consumption of Mg-MOF-74 (2.2–2.3 MJ/kg CO_2) [89]. Notably, the energy requirement was reduced by approximately 10–20% through synergies with light.

Because of the excellent performance of azo-derived modified MOFs in light-response desorption of CO_2 and separation of alkane pollutants, a series of azo-derived modified MOFs were developed for adsorption and light-response desorption studies [47,75]. However, the azo-derived heterogeneous process was often limited by UV light excitation. UV light is well known for breaking down organic molecules, and the photoisomerization process needs to activate the light conversion reaction, which substantially limits the broad application of light-controlled, intelligent materials. The nondestructive nature of near-infrared wavelength light has a great practical application prospect for the loading and directional photoinduced release of medical drugs [90]. Therefore, photoisomerization induced by visible light has attracted extensive research attention. By designing the azo ligands, smart MOFs with photoisomerization under visible light conditions have been obtained. According to previous reports, changing the electron distribution near and around azo bonds or adjusting the degree of bulkiness of the pendant ligand can affect the wavelength of the switch, the integrity of the switching, and/or the amount of blocking around the metal clusters or pores [91]. However, such studies are insufficient thus far, and similar investigations are still warranted to understand the visible light-response adsorption and desorption process; introducing highly electronegative fluorine atoms to the central azo bond may affect the electron distribution near and around azo bonds or adjust the degree of bulkiness of the pendant ligand and adjust the response wavelength of the switching [91,92].

Using difluoronated azo derivatives as ligands, Knebel et al. [92] designed a photoisomerized MOF $Cu_2(F_2azoBDC)_2(dabco)$, which has switching behavior after being exposed to green or violet light. In addition, visible light can increase the isomerization yields by avoiding the competition with LMCT resulting from UV light in Cu-paddle-wheel structures. The $Cu_2(F_2azoBDC)_2(dabco)$ film on mesoporous Al_2O_3 supports could separate H_2/hydrocarbon mixtures while failing to separate the H_2/CO_2 matrix. Therefore, the modulation of H_2/hydrocarbon separation upon visible light irradiation was used to tap the pore opening/blocking effects of the *cis–trans* isomers of F_2azoBDC.

Modifying MOFs with azo dyes is also an effective approach to constructing light-responsive MOFs. Ladewig et al. [93] introduced methyl red (MR) to modify Mg-MOF-74 and MIL-53 (Al) to adsorb CO_2 after exposure to visible light. MR-modified Mg-MOF-74 can achieve 84% uptake change upon visible light irradiation due to the low-energy alternative for CO_2 adsorption.

2.1. Photoreactive molecular switch MOFs

Another promising strategy for constructing light-responsive MOFs is to attach a photoreactive molecular switch onto the open metal sites of the MOFs. Luo and coworkers [36] developed a distinct strategy for constructing a diarylethene Zn(L)-(bpdc)·solvents (L = diarylethene; H_2bpdc = biphenyl-4,4′-dicarboxylic acid). As shown in Fig. 9a, the diarylethene derivative unit displayed open-ring and closed-ring isomer responses under UV and visible light, respectively. Generally, the photoisomerization of diarylethene derivatives is produced from the mutual transformation of its structure between open-ring and closed-ring forms.

The single crystal of Zn(L)-(bpdc)·solvents appeared blue under UV irradiation but orange under visible light, which might originate from the photoisomerism of the L ligand (Fig. 9b). A similar change in the UV–vis absorption spectrum further confirmed this hypothesis (Fig. 9c). Zn(L)-(bpdc)·solvents showed a similar CO_2 desorption capacity (75–76%)

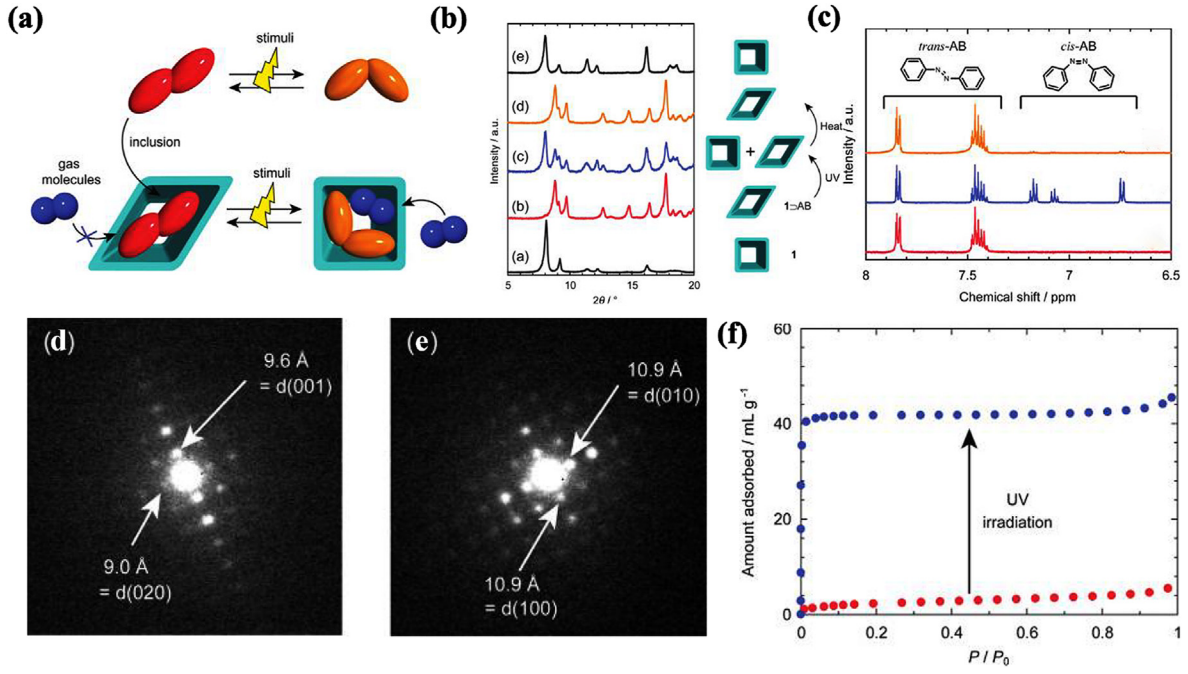

Fig. 10. (a) Schematic illustration of *trans*–AB and *cis*–AB under different light stimulation conditions; (b) the XRD patterns of **1**, **1**⊃AB, **1**⊃AB(UV), solid **1**⊃AB(UV) (after heating at 120 °C), and the adduct of **1** with *cis*–stilbene; (c) ^{1}H NMR spectra of CD_2Cl_2 solutions of AB isolated from **1**⊃AB, **1**⊃AB(UV), and the solid **1**⊃AB(UV) (after heating at 120 °C); electron-beam diffraction patterns in a TEM for single particles of (d) **1**⊃AB and (e) **1**⊃AB(UV); (f) the N_2 adsorption isotherms of **1**⊃AB and **1**⊃AB(UV) at 77 K. Reprinted with permission from Ref. [33] (Copyright 2012 American Chemical Society).

under static and dynamic irradiation, respectively (Fig. 9d and e). Interestingly, Zn(L)-(bpdc)·solvents showed a very large adsorption capacity for CO_2 when exposed to UV light (20.1 cm^3/g, 298 K), which was 4-fold greater than the adsorption capacity under the same conditions without UV irradiation (5.0 cm^3/g, 298 K). The PXRD patterns and TGA experiments were used to investigate whether the skeleton was well retained after the UV and visible light irradiation. The results revealed that even after being heated at 300 °C, the skeleton was still well maintained, implying that no noticeable framework expansion, reduction, or XRD peak shift occurred during structural transformation. The authors also carried out an in situ dynamic CO_2-adsorption experiment to investigate the CO_2 release under ambient conditions. In the experiment, the adsorption and desorption segments were performed under UV irradiation and ambient light, respectively. Under these conditions, a 24% desorption capacity was observed. The results demonstrated that the CO_2 desorption capacity of Zn(L)-(bpdc)·solvents was modulated under distinct triggers.

2.2. MOFs with light-responsive guests

A change in guest molecule structure might lead to a change in the host crystal framework [32]. Loading the photo-responsive heterogeneous guest molecules with suitable size into the flexible MOF framework is also an effective strategy for achieving light-response desorption and desorption [33]. Kitagawa et al. [33] constructed a host-guest transmission system by packing the *trans*-azo (AB) into flexible MOFs $[Zn_2(terephthalate)_2(triethylenediamine)]_n$ (**1**) to form a composite of **1**⊃AB at 120 °C (Fig. 10a). Using the Le Bail fitting analysis of the PXRD data, the crystal structure changed from the original square of the pristine **1** to a diamond of the as-prepared **1**⊃AB (Fig. 10b). In **1**⊃AB, a stretching vibration peak at 690 cm^{-1} in the FTIR spectra was detected, which was ascribed to *trans*–AB [94]. After UV irradiation, the FTIR spectrum of **1**⊃AB displayed the characteristic *cis*–isomer peaks of AB at 697 nm, indicating that the isomerization occurred under ultraviolet light. No characteristic peaks of *cis*–AB were present in the FTIR and ^1H NMR spectra of **1**⊃AB before UV irradiation, indicating that the AB in **1**⊃AB basically exists as the *trans*–isomer before UV irradiation. The ^1H NMR spectrum was used to quantify the *cis*–*trans* isomer ratio (38:62) of AB after UV irradiation (Fig. 10c). TEM results indicated that the diffraction pattern of the particle from **1**⊃AB is due to the orthogonal form of host **1**, and the transformation of the host structure occurred in the entire particle rather than the crystalline part of the particle (Fig. 10d and e). As shown in Fig. 10f, **1**⊃AB hardly adsorbed N_2 in the absence of UV radiation, while the adsorption capacity of **1**⊃AB toward N_2 after UV radiation was 45 mL/g. According to previous reports, when AB was combined with the rigid mesoporous material, AB isomerism did not affect the N_2 adsorption capacity [33,95,96]. Therefore, the main factor causing the change in N_2 adsorption capacity was AB isomerism leading to a change in the N_2 host structure. After a treatment at 120 °C, the adsorption capacity of the **1**⊃AB (UV) pair of nitrogen was substantially reduced, indicating that bidirectional control of N_2 adsorption performance was achieved by external stimulation. This methodology provides a simple and efficient way to combine flexible MOFs with a variety of stimulus-response molecules to construct a variety of unconventional, smart, and porous materials.

Diarylethene (1,2-bis(2,5-dimethyl-thien-3-yl)-perfluorocyclopentene, DTE) is a molecule with good spectral response, thermal stability, and excellent distinct spectral response [97]. Under UV and visible light conditions, the structure of DTE appeared to be closed and open, and its color was red and colorless, respectively. Benedict et al. [97] reported the first MOF $[Zn_2(terephthalate)_2(triethylenediamine)]_n$-attached DTE (DMOF-1) as guest molecules. DMOF-1 appeared red under UV irradiation. However, once the UV irradiation stopped and the visible light irradiation opened, DMOF-1 returned to colorless. Common light-responsive guest molecules are summarized in Scheme 1.

Hill and coworkers [49] prepared an optical fiber coated with stable UiO-66, in which a sublimation method was developed to encapsulate 5-fluorouracil (5-FU) into the pores of dense UiO-66 film. The 5-FU wrapped in the optical fiber UiO-66 film can realize the directional desorption of 5-FU under the trigger of the light from the optical fiber (Fig. 11a). The optical fiber was obtained by impregnating the fiber into a precursor solution of UiO-66. Scanning electron microscopy (SEM) of the terminal face of optical fiber film indicated that the thickness of the UiO-66 film is between 1.6 and 2 μm (Fig. 11b). The intermolecular forces between UiO-66 and 5-FU involved hydrogen bonding and π-π interactions. Dispersion-corrected semi-empirical DFT-D2 modeling and calculations were introduced to judge the optimized location of 5-FU within UiO-66. The simulation results revealed that the preferential

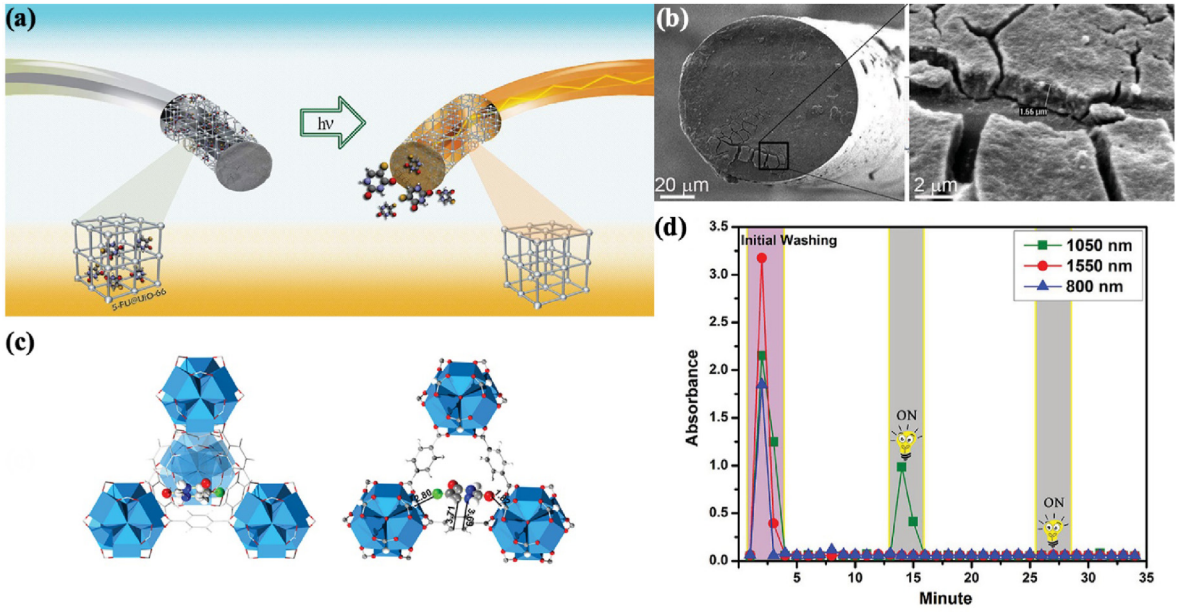

Fig. 11. (a) Schematic of 5-FU encapsulation into fiber coated with UiO-66 and a photoinduced drug delivery system; (b) SEM images of the terminal face of an optical fiber coated with UiO-66; (c) DFT-D2 optimized location of 5-FU in the pore structure of UiO-66 and the interaction distance between 5-FU and UiO-66; (d) absorbance of solution around UiO-66 optical fiber film at 265 nm under different wavelengths of light. Reprinted with permission from Ref. [49] (Copyright 2016 WILEY-VCH).

positions were located around the triangular pore window of the tetrahedral cage, followed by octahedral cages (Fig. 11c) [99,100]. The pore size distribution alteration of unmodified UiO-66 and 5-FU-loaded UiO-66 confirmed that 5-FU was anchored mostly into the tetrahedral cages and partly into the octahedral cages. The release of 5-FU into the solution was studied using light of different wavelengths (Fig. 11d). According to density functional theory (DFT) calculations, the binding energy of 5-FU and UiO-66 is approximately 100 kJ/mol, being equivalent to 1197-nm light. No 5-FU release was found upon irradiation with wavelengths of 800 and 1550 nm. By changing the wavelength to 1050 nm, UiO-66 containing 5-FU was sufficiently activated to exceed the adsorption enthalpy between 5-FU and UiO-66 to accomplish the in situ 5-FU adsorption. Approximately 1.10×10^{-4} M of 5-FU can be delivered within 60 s from one fiber coated with UiO-66, in which the light with a suitable wavelength through the fiber could trigger 5-FU desorption as a new approach to localized drug administration. This study provided an ingenious way to load the cancer drug 5-FU into porous UiO-66 using light as a trigger to deliver the cancer drug on demand.

2.3. MOF composites

Compositing light-sensitive nanoparticles (NPs) on the surface of MOFs also realized light-control adsorption/desorption of the target pollutants. Ag_3PO_4 NPs as a semiconductor photocatalyst exhibited excellent photooxidative capabilities under visible light irradiation [101,102], suffering photo-corrosion by the photogenerated electrons [103], and the Ag^+ ions in Ag_3PO_4 NPs were reduced to Ag^0 (Eq. (1)) [101,104].

$$4Ag_3PO_4 + 6H_2O + 12h^+ + 12e^- \rightarrow 12Ag + 4H_3PO_4 + 3O_2 \quad (1)$$

Wang and coworkers [47] first proposed an in situ deposition/precipitation approach to fabricating UiO-66-NH_2/Ag_3PO_4 composites for light-stimuli desorption of SMX (UAP-X, X represents a

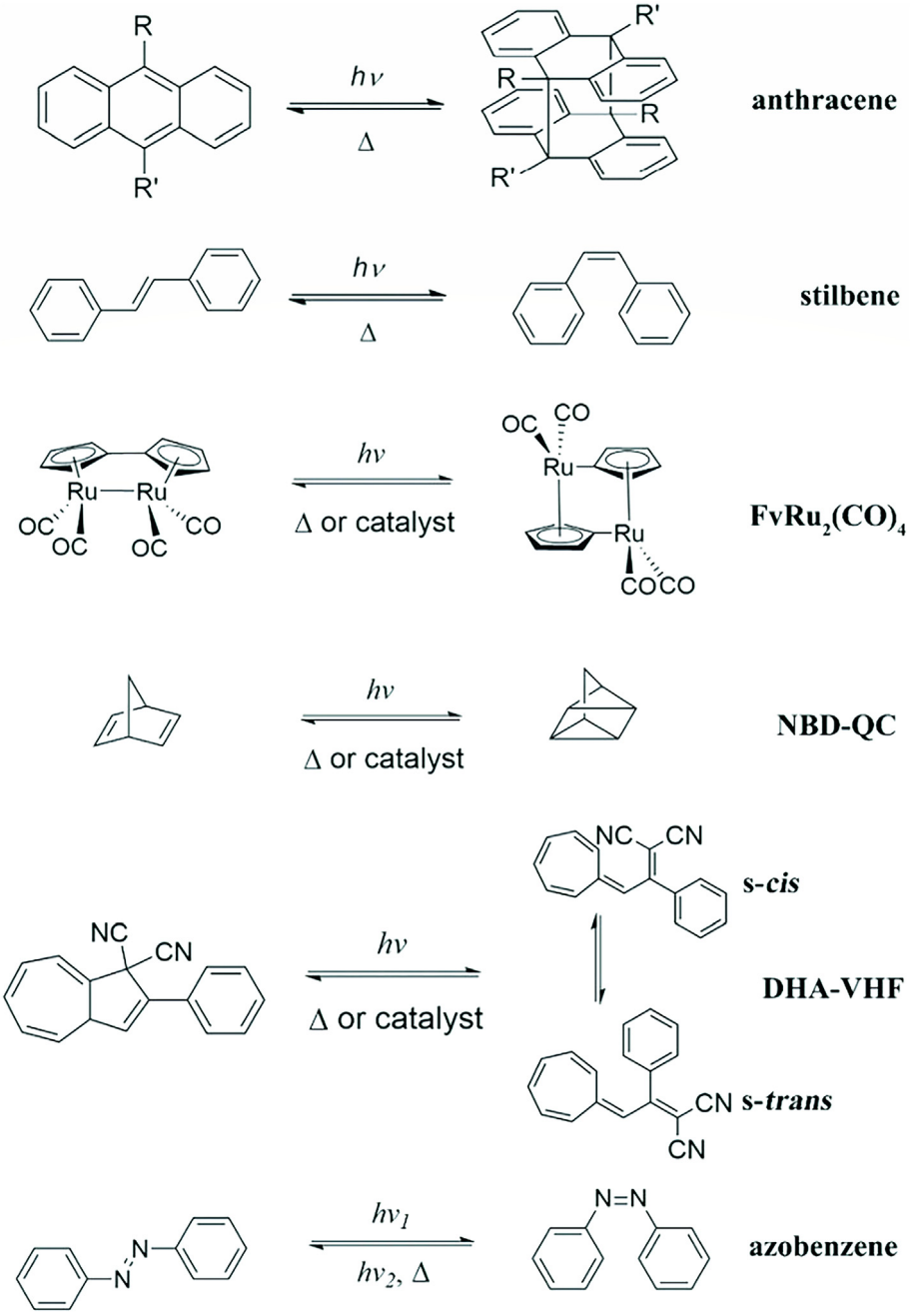

Scheme. 1. Types of photoisomerized molecules. Reprinted with permission from [98] (Copyright 2018 Royal Society of Chemistry).

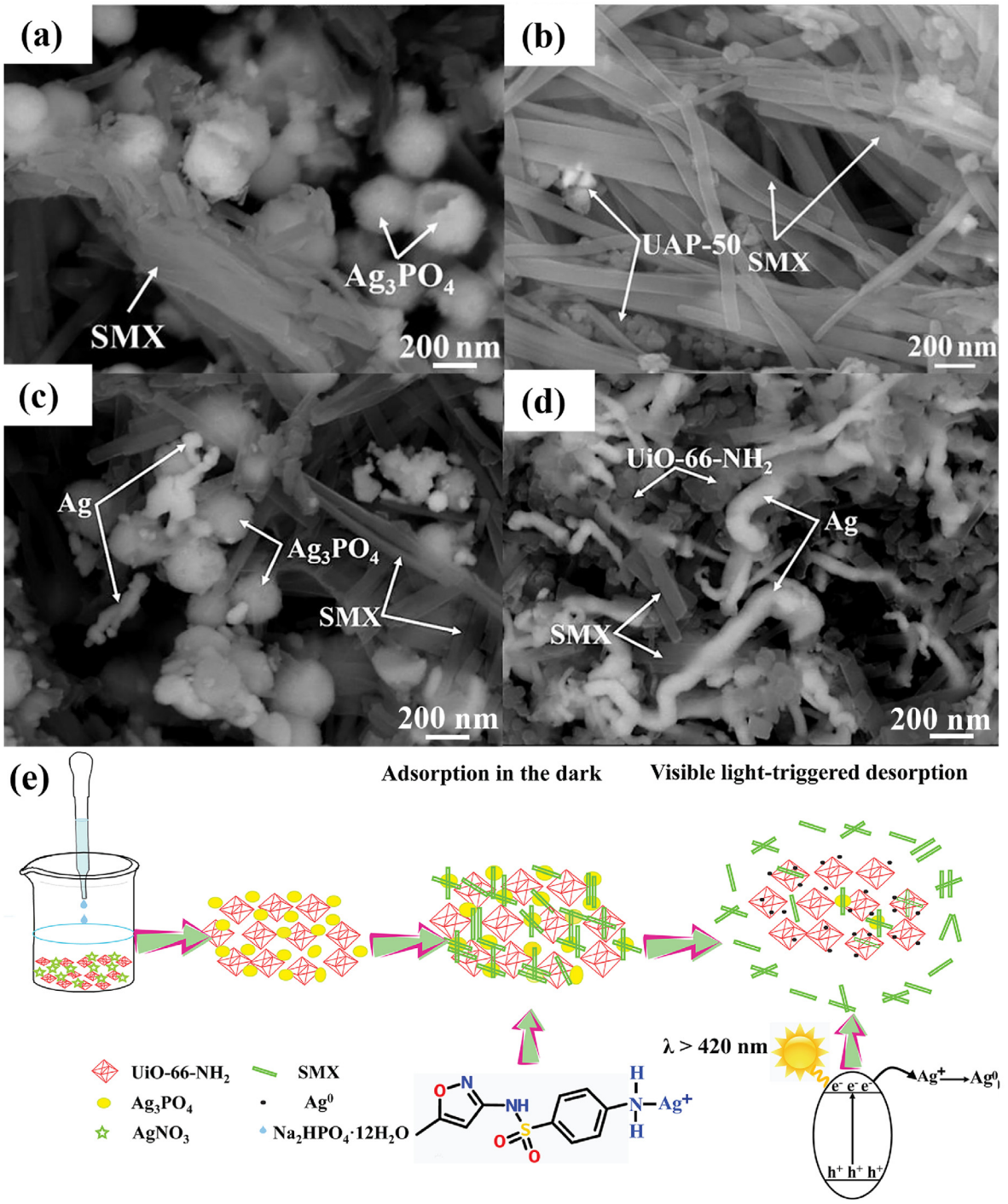

Fig. 12. SEM images of (a) Ag_3PO_4; (b) UAP-50 after adsorption of SMX; and (c) Ag_3PO_4; (d) UAP-50 after desorption of SMX by visible light. (e) Adsorption and desorption mechanisms of UAP-50 toward SMX. Reprinted with permission from Ref. [47] (Copyright 2018 Elsevier).

$UiO-66-NH_2$ mass of 20, 35, 50, 120, and 200 mg in the composites). The results indicated that the individual Ag_3PO_4 and $UiO-66-NH_2$ MOFs did not perform light-triggered desorption activity toward SMX. However, once $UiO-66-NH_2$ was introduced into Ag_3PO_4, UAP-X showed obvious light-triggered desorption behavior toward SMX. SMX adsorption and desorption test results indicated that UAP-50/120 performed excellent desorption activities under visible light (about 66.9/73%).

Compared with Ag_3PO_4 NPs, the characteristic PXRD diffraction peaks (38.11°, 44.30°, 64.44°, 77.39°, and 81.54°) of Ag^0 appeared in the UAP-50 spectrum after light-triggered desorption. Furthermore, the SEM images of Ag_3PO_4 and UAP-50 with SMX adsorption showed strip-like SMX, indicating the successful adsorption of SMX (Fig. 12a and b). As illustrated in Fig. 12c and d, more Ag^0 appeared on the surface of SMX@UAP-50 than on the surface of SMX@Ag_3PO_4 upon visible light irradiation for 2 h, indicating that introducing $UiO-66-NH_2$ promoted the reduction of Ag^+. In addition, the XPS peaks (374.6 and 368.6 eV) of Ag^0 appeared in the UAP-50 spectrum with SMX adsorption after visible light irradiation. Therefore, the conclusion was drawn that the light-triggered desorption activity of UAP-X composites might be due to the reduction of Ag^+ in Ag_3PO_4 NPs to the element Ag^0 under visible light irradiation

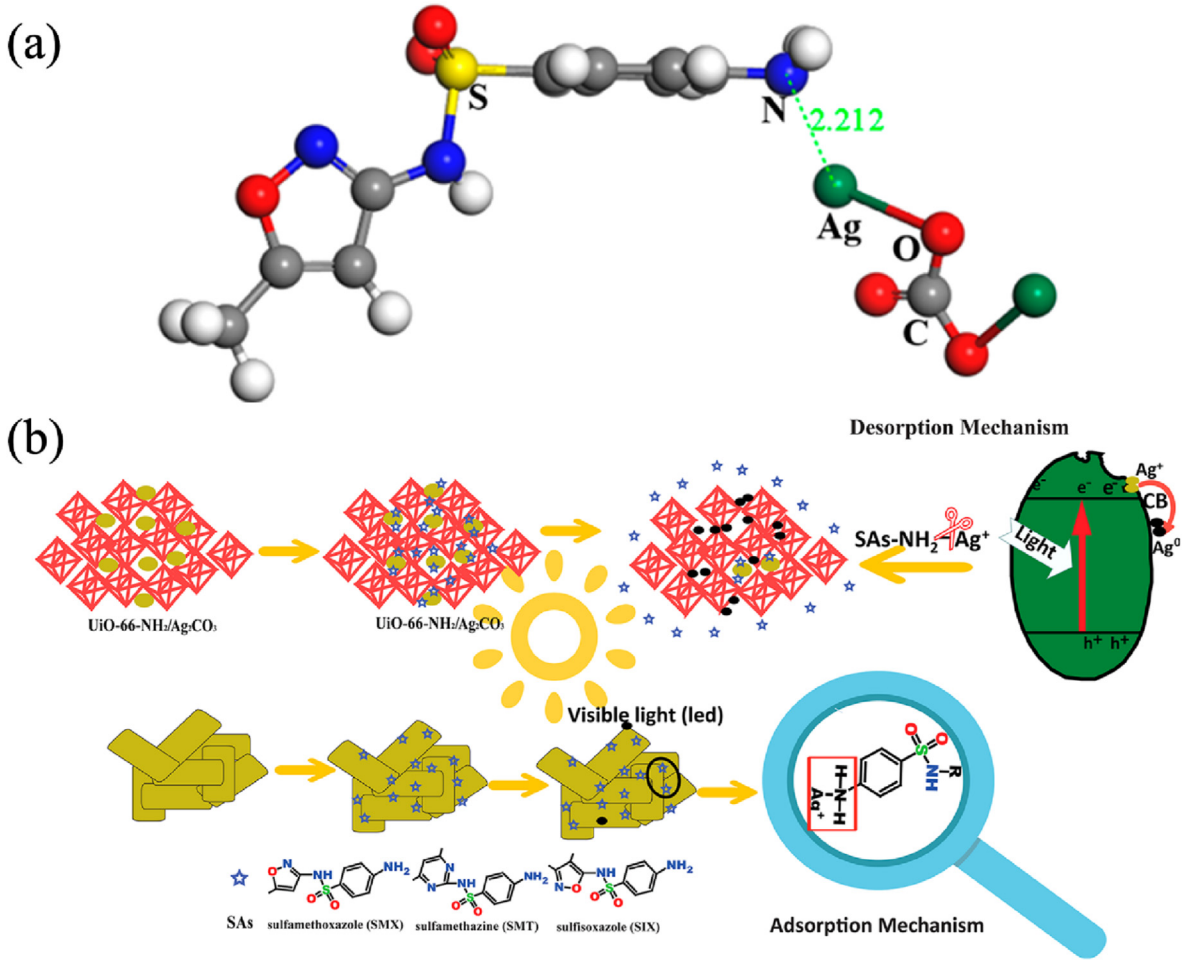

Fig. 13. (a) DFT calculation models for the optimal coordination of $–NH_2$ and Ag^+; (b) desorption mechanism of UAP-X composites toward SAs under visible light. Reprinted with permission from Ref. [44] (Copyright 2018 American Chemical Society).

(Fig. 12e) [104,105].

Ag_3PO_4, Ag_3VO_4, Ag_2CrO_4, and Ag_2CO_3 are well known for possessing excellent photosensitive performance, in which Ag^+ can be converted to Ag^0 under light irradiation [106,107]. Wang and coworkers [44] further fabricated UiO-66-NH_2/Ag_2CO_3 (UAC-X) composites for visible-light-controlled release of different sulfonamides (SAs), such as sulfamethoxazole (SMX), sulfisoxazole (SIX), and sulfamethazine (SMT). The results indicated that UAC-150 performed good dark adsorption activities and excellent desorption toward various SAs upon visible light illumination (with desorption efficiencies of 80.8% for SMX, 66.7% for SIX, and 43.7% for SMT). The desorption performance of UAC-X composites toward SMX was controlled by the mass content of UiO-66-NH_2 in the UAC-X composites. As the content of UiO-66-NH_2 increased, the desorption ratio of SMX increased from 0% for UAC-20 to 80.8% for UAC-150 under the same condition. The corresponding desorption rate was also positively correlated with the content of UiO-66-NH_2. This phenomenon is observed because SMX wrapped on UAP-X composites prevents these composites from obtaining light, thus inhibiting the conversion of Ag^+ to Ag^0. Furthermore, increasing the proportion of UiO-66-NH_2 in UAC-X composites was found to reduce the particle size of Ag_2CO_3. The smaller size of Ag_2CO_3 NPs accomplished stronger light-capturing capability and accelerated the reduction activity of Ag^+. An analysis of XPS, TEM, and FTIR results shows that SMX was successfully adsorbed on UAC-X composites, in which the adsorption mechanism contributed to the coordination interaction between Ag^+ in Ag_2CO_3 NPs and $–NH_2$ in SMX. A DFT calculation revealed that the adsorption activity of UAC-X toward SMX was primarily chemical adsorption (bonding energy = −0.925 eV) (Fig. 13a). The E_g value of Ag_2CO_3 was 2.3 eV [108], indicating that the photoinduced electron process can be accomplished under light with a wavelength below 539 nm [44]. The light-triggered desorption process can be explained as the reduction of Ag^+ in UAC-X composites to Ag^0 by capturing photogenerated electrons under visible light excitation, resulting in the breaking of the interaction between $–NH_2$ (SAs) and Ag^+ (UAC-X composites) (Fig. 13b). This work provides a new strategy for applying light-response desorption materials in a water environment, further broadening the applicability of the composite material based on a silver salt semiconductor and UiO-66-NH_2 as an effective photocontrolled adsorption–desorption material for sulfonamide antibiotics, and it provides a new path for photocontrolled drug delivery and environmental pretreatment.

3. Conclusion

In conclusion, the design strategy, light-operated methods, and potential applications of light-response MOFs were discussed. The different strategies of light-response adsorption and desorption were classified and compared. The full realization of their potential anticipates a bright future in adsorption, controlled release, and drug delivery. The opportunities provided by light-response MOFs have been summarized for future applications in gas adsorption, catalysis, optical, and biomedical applications. The future development directions of optical response MOFs should target the following aspects. (i) It is essential to design and synthesize the third generation of light-responsive MOFs, which can alter

the characteristics of the pore size and pore shape for smart adsorption and desorption of targeted molecules. (ii) Developing visible and/or near-infrared light-responsive adsorption–desorption MOF materials is necessary to achieve practical applications. (iii) The light-response adsorption and desorption performance and mechanism of light-responsive MOFs in an aqueous environment must be explored for wastewater purification and sample pretreatment. (iv) Light-response MOFs can be combined with other stimulus-response switches (such as magnetism, temperature, pressure, etc.) to achieve the synergistic effect of multiple stimuli. Furthermore, many challenges, including environmental tolerance, physiological toxicity, physiological compatibility, the construction of practical devices, and their use in practical engineering, need to be addressed. Further developments of light-response MOFs will play important roles in the field of smart materials.

Declaration of competing interest

The authors declare that they have no known competing financial interests or personal relationships that could have appeared to influence the work reported in this paper.

Acknowledgements

This work was supported by the National Natural Science Foundation of China (51878023), the Fundamental Research Funds for Beijing University of Civil Engineering and Architecture (X20147/X20141/X20135/X20146) and BUCEA Post Graduate Innovation Project (2022).

References

[1] H.C. Gulbalkan, Z.P. Haslak, C. Altintas, A. Uzun, S. Keskin, Assessing CH_4/N_2 separation potential of MOFs, COFs, IL/MOF, MOF/polymer, and COF/polymer composites, Chem. Eng. J. 428 (2022) 131239.
[2] J. Wang, A.S. Cherevan, C. Hannecart, S. Naghdi, S.P. Nandan, T. Gupta, D. Eder, Ti-based MOFs: new insights on the impact of ligand composition and hole scavengers on stability, charge separation and photocatalytic hydrogen evolution, Appl. Catal. B Environ. 283 (2021) 119626.
[3] H. Daglar, H.C. Gulbalkan, G. Avci, G.O. Aksu, O.F. Altundal, C. Altintas, I. Erucar, S. Keskin, Effect of metal–organic framework (MOF) database selection on the assessment of gas storage and separation potentials of MOFs, Angew. Chem. Int. Ed. 60 (2021) 7828–7837.
[4] R. Sahoo, M.C. Das, C_{2s}/C_1 hydrocarbon separation: the major step towards natural gas purification by metal–organic frameworks (MOFs), Coord. Chem. Rev. 442 (2021) 213998.
[5] Y.H. Li, C.C. Wang, X. Zeng, X.Z. Sun, C. Zhao, H. Fu, P. Wang, Seignette salt induced defects in Zr-MOFs for boosted Pb(II) adsorption: universal strategy and mechanism insight, Chem. Eng. J. 442 (2022) 136276.
[6] X. Ren, C.C. Wang, Y. Li, C.Y. Wang, P. Wang, S. Gao, Ag(I) removal and recovery from wastewater adopting NH_2-MIL-125 as efficient adsorbent: a 3Rs (reduce, recycle and reuse) approach and practice, Chem. Eng. J. 442 (2022) 136306.
[7] X.H. Yi, H. Ji, C.C. Wang, Y. Li, Y.H. Li, C. Zhao, A. Wang, H. Fu, P. Wang, X. Zhao, W. Liu, Photocatalysis-activated SR-AOP over PDINH/MIL-88A(Fe) composites for boosted chloroquine phosphate degradation: performance, mechanism, pathway and DFT calculations, Appl. Catal. B Environ. 293 (2021) 120229.
[8] Q. Zhao, X.H. Yi, C.C. Wang, P. Wang, W. Zheng, Photocatalytic Cr(Vl) reduction over MIL-101(Fe)-NH_2 immobilized on alumina substrate: from batch test to continuous operation, Chem. Eng. J. 429 (2022) 132497.
[9] Q. Zhao, C.C. Wang, P. Wang, Effective norfloxacin elimination via photo-Fenton process over the MIL-101(Fe)-NH_2 immobilized on α-Al_2O_3 sheet, Chin. Chem. Lett. (2022), https://doi.org/10.1016/j.cclet.2022.01.033.
[10] S. Ma, D. Sun, D. Yuan, X.S. Wang, H.C. Zhou, Preparation and gas adsorption studies of three mesh-adjustable molecular sieves with a common structure, J. Am. Chem. Soc. 131 (2009) 6445–6451.
[11] D. Zhao, D.Q. Yuan, R. Krishna, J.M. van Baten, H.C. Zhou, Thermosensitive gating effect and selective gas adsorption in a porous coordination nanocage, Chem. Commun. 46 (2010) 7352–7354.
[12] T.D. Nguyen, Y. Liu, S. Saha, K.C.F. Leung, J.F. Stoddart, J.I. Zink, Design and optimization of molecular nanovalves based on redox-switchable bistable rotaxanes, J. Am. Chem. Soc. 129 (2007) 626–634.
[13] T.D. Nguyen, H.R. Tseng, P.C. Celestre, A.H. Flood, Y. Liu, J.F. Stoddart, J.I. Zink, A reversible molecular valve, Proc. Natl. Acad. Sci. Unit. States Am. 102 (2005) 10029–10034.
[14] C. Park, K. Oh, S. Lee, C. Kim, Controlled release of guest molecules from mesoporous silica particles based on a pH-responsive polypseudorotaxane motif, Angew. Chem. Int. Ed. 46 (2007) 1455–1457.
[15] S. Angelos, Y.W. Yang, N.M. Khashab, J.F. Stoddart, J.I. Zink, Dual-controlled nanoparticles exhibiting and logic, J. Am. Chem. Soc. 131 (2009) 11344–11346.
[16] B. John-Christopher, C. Carl-Johan, B.D. Gates, N.R. Branda, Two-way photoswitching using one type of near-infrared light, upconverting nanoparticles, and changing only the light intensity, J. Am. Chem. Soc. 132 (2010) 15766–15772.
[17] S. Yagai, A. Kitamura, Recent advances in photoresponsive supramolecular self-assemblies, Chem. Soc. Rev. 37 (2008) 1520–1529.
[18] D.P. Ferris, Y.L. Zhao, N.M. Khashab, H.A. Khatib, J.F. Stoddart, J.I. Zink, Light-operated mechanized nanoparticles, J. Am. Chem. Soc. 131 (2009) 1686–1688.
[19] Q.L. Zhu, T.L. Sheng, R.B. Fu, S.M. Hu, L. Chen, C.J. Shen, X. Ma, X.T. Wu, Redox-responsive photochromism and fluorescence modulation of two 3D metal–organic hybrids derived from a triamine-based polycarboxylate ligand, Chem. Eur J. 17 (2011) 3358–3362.
[20] S. Sortino, Photoactivated nanomaterials for biomedical release applications, J. Mater. Chem. 22 (2012) 301–318.
[21] Y. Wei, S. Han, J. Kim, S. Soh, B.A. Grzybowski, Photoswitchable catalysis mediated by dynamic aggregation of nanoparticles, J. Am. Chem. Soc. 132 (2010) 11018–11020.
[22] Y. Shiraishi, K. Tanaka, E. Shirakawa, Y. Sugano, S. Ichikawa, S. Tanaka, T. Hirai, Light-triggered self-assembly of gold nanoparticles based on photoisomerization of spirothiopyran, Angew. Chem. Int. Ed. 52 (2013) 8304–8308.
[23] S. Zhang, Y. Peng, W. Jiang, X. Liu, X. Song, B. Pan, H.Q. Yu, Light-triggered reversible sorption of azo dyes on titanium xerogels with photo-switchable acetylacetonato anchors, Chem. Commun. 50 (2014) 1086–1088.
[24] W.G. Becker, A.J. Bard, Photoluminescence and photoinduced oxygen adsorption of colloidal zinc sulfide dispersions, J. Phys. Chem. 87 (1983) 4888–4893.
[25] X.Y. Zhu, S.R. Hatch, A. Campion, J.M. White, Surface photochemistry. II. Wavelength dependences of photoinduced dissociation, desorption, and rearrangement of O_2 on Pt(111), J. Chem. Phys. 91 (1989) 5011–5020.
[26] B. Hellsing, D.V. Chakarov, L. Österlund, V.P. Zhdanov, B. Kasemo, Photoinduced desorption of potassium atoms from a two dimensional overlayer on graphite, J. Chem. Phys. 106 (1997) 982–1002.
[27] N. Chakrabarti, N. Sathyamurthy, J.W. Gadzuk, Photoinduced desorption of molecules from metal surfaces using femtosecond pulses: a model dynamical study, J. Phys. Chem. 102 (1998) 4154–4157.
[28] H. Tada, K. Teranishi, S. Ito, H. Kobayashi, S. Kitagawa, H_2 generation by cycling dark adsorption and successive photoinduced desorption of 2-mercaptopyridine on/from Ag-core/Pt-shell nanoparticles loaded on TiO_2, Langmuir 16 (2000) 6077–6080.
[29] C. Feng, J. Zhang, R. Lang, Z. Jin, Z. Wu, Z. Zhang, Unusual photo-induced adsorption-desorption behavior of propylene on Ag/TiO_2 nanotube under visible light irradiation, Appl. Surf. Sci. 257 (2011) 1864–1870.
[30] U. Mueller, M. Schubert, F. Teich, H. Puetter, K. Schierle-Arndt, J. Pastré, Metal–organic frameworks-prospective industrial applications, J. Mater. Chem. 16 (2006) 626–636.
[31] A.A. Olajire, Synthesis chemistry of metal–organic frameworks for CO_2 capture and conversion for sustainable energy future, Renew. Sustain. Energy Rev. 92 (2018) 570–607.
[32] J.J. Li, C.C. Wang, H.F. Fu, J.R. Cui, P. Xu, J. Guo, J.R. Li, High-performance adsorption and separation of anionic dyes in water using a chemically stable graphene-like metal–organic framework, Dalton Trans. 46 (2017) 10197–10201.
[33] N. Yanai, T. Uemura, M. Inoue, R. Matsuda, T. Fukushima, M. Tsujimoto, S. Isoda, S. Kitagawa, Guest-to-host transmission of structural changes for stimuli-responsive adsorption property, J. Am. Chem. Soc. 134 (2012) 4501–4504.
[34] Z. Zhou, M. Vázquez-González, I. Willner, Stimuli-responsive metal–organic framework nanoparticles for controlled drug delivery and medical applications, Chem. Soc. Rev. 50 (2021) 4541–4563.
[35] X. Chai, H.H. Hao, A.C. Sedgwick, N. Li, Y. Zang, T.D. James, J. Zhang, X.H. Hu, Y. Yu, Y. Li, Y. Wang, J. Li, X.P. He, H. Tian, Photochromic fluorescent probe strategy for the super-resolution imaging of biologically important biomarkers, J. Am. Chem. Soc. 142 (2020) 18005–18013.
[36] F. Luo, C.B. Fan, M.B. Luo, X.L. Wu, Y. Zhu, S.Z. Pu, W.Y. Xu, G.C. Guo, Photoswitching CO_2 capture and release in a photochromic diarylethene metal–organic framework, Angew. Chem. Int. Ed. 126 (2014) 9452–9455.
[37] A.B. Kanj, K. Müller, L. Heinke, Stimuli-responsive metal–organic frameworks with photoswitchable azobenzene side groups, Macromol. Rapid Commun. 39 (2018) 1700239.
[38] H. Li, M.R. Martinez, Z. Perry, H.C. Zhou, P. Falcaro, C. Doblin, S. Lim, A.J. Hill, B. Halstead, M.R. Hill, A robust metal–organic framework for dynamic light-induced swing adsorption of carbon dioxide, Chem. Eur J. 22 (2016) 11176–11179.
[39] F.X. Coudert, Responsive metal–organic frameworks and framework materials: under pressure, taking the heat, in the spotlight, with friends, Chem. Mater. 27 (2015) 1905–1916.
[40] R. Lyndon, K. Konstas, B.P. Ladewig, P.D. Southon, P.C.J. Kepert, M.R. Hill, Dynamic photo-switching in metal–organic frameworks as a route to low-energy carbon dioxide capture and release, Angew. Chem. Int. Ed. 52 (2013) 3695–3698.
[41] J. Park, D. Yuan, K.T. Pham, J.R. Li, A. Yakovenko, H.C. Zhou, Reversible alteration of CO_2 adsorption upon photochemical or thermal treatment in a metal–organic framework, J. Am. Chem. Soc. 134 (2012) 99–102.
[42] Y.G. Liu, G. Liu, P. Tan, C. Gu, J.J. Li, X.Q. Liu, L.B. Sun, Near-infrared light triggered release of ethane from a photothermal metal–organic framework, Chem. Eng. J. 420 (2021) 130490.
[43] J.K. Wu, P. Tan, J. Lu, Y. Jiang, X.Q. Liu, L.B. Sun, Fabrication of photothermal silver nanocube/ZIF-8 composites for visible-light-regulated release of propylene, ACS Appl. Mater. Interfaces 11 (2019) 29298–29304.

[44] X.Y. Xu, J. Zhang, X. Z, H. Fu, C. Chu, P. Wang, C.C. Wang, Visible-light-triggered release of sulfonamides in MOF/Ag-based nanoparticle composites: performance, mechanism, and DFT calculations, ACS Appl. Nano Mater. 2 (2019) 418–428.

[45] H. Liu, N. Li, M. Feng, G. Li, W. Zhang, T. An, Near-infrared light induced adsorption-desorption cycle for VOC recovery by integration of metal–organic frameworks with graphene oxide nanosheets, Environ. Sci.: Nano (2022), https://doi.org/10.1039/D2EN00103A.

[46] H. Li, M.M. Sadiq, K. Suzuki, C. Doblin, S. Lim, P. Falcaro, A.J. Hill, M.R. Hill, MaLISA—a cooperative method to release adsorbed gases from metal–organic frameworks, J. Mater. Chem. 4 (2016) 18757–18762.

[47] X.Y. Xu, C. Chu, H. Fu, X.D. Du, P. Wang, W. Zheng, C.C. Wang, Light-responsive UiO-66-NH_2/Ag_3PO_4 MOF-nanoparticle composites for the capture and release of sulfamethoxazole, Chem. Eng. J. 350 (2018) 436–444.

[48] X. Meng, B. Gui, D. Yuan, M. Zeller, C. Wang, Mechanized azobenzene-functionalized zirconium metal–organic framework for on-command cargo release, Sci. Adv. 2 (2016) e1600480.

[49] M. Nazari, M. Rubio-Martinez, G. Tobias, J.P. Barrio, R. Babarao, F. Nazari, K. Konstas, B.W. Muir, S.F. Collins, A.J. Hill, M.C. Duke, M.R. Hill, Metal–organic framework-coated optical fibers as light-triggered drug delivery vehicles, Adv. Funct. Mater. 26 (2016) 3244–3249.

[50] K. Müller, A. Knebel, F. Zhao, D. Bléger, J. Caro, L. Heinke, Switching thin films of azobenzene-containing metal–organic frameworks with visible light, Chem. Eur J. 23 (2017) 5434–5438.

[51] J.W. Brown, B.L. Henderson, M.D. Kiesz, A.C. Whalley, W. Morris, S. Grunder, H. Deng, H. Furukawa, J.I. Zink, J.F. Stoddart, O.M. Yaghi, Photophysical pore control in an azobenzene-containing metal–organic framework, Chem. Sci. 4 (2013) 2858–2864.

[52] A. Modrow, D. Zargarani, R. Herges, N. Stock, The first porous MOF with photoswitchable linker molecules, Dalton Trans. 40 (2011) 4217–4222.

[53] B.J. Furlong, M.J. Katz, Bistable dithienylethene-based metal–organic framework illustrating optically induced changes in chemical separations, J. Am. Chem. Soc. 139 (2017) 13280–13283.

[54] Z. Wang, A. Knebel, S. Grosjean, D. Wagner, S. Bräse, C. Wöll, J. Caro, L. Heinke, Tunable molecular separation by nanoporous membranes, Nat. Commun. 7 (2016) 13872.

[55] L.L. Gong, X.F. Feng, F. Luo, X.F. Yi, A.M. Zheng, Removal and safe reuse of highly toxic allyl alcohol using a highly selective photo-sensitive metal–organic framework, Green Chem. 18 (2016) 2047–2055.

[56] R. Lyndon, K. Konstas, B.P. Ladewig, P.D. Southon, C.J. Kepert, M.R. Hill, Rücktitelbild: dynamic photo-switching in metal–organic frameworks as a route to low-energy carbon dioxide capture and release, Angew. Chem. Int. Ed. 125 (2013) 3864–3864.

[57] F. Bigdeli, C.T. Lollar, A. Morsali, H.C. Zhou, Switching in metal–organic frameworks, Angew. Chem. Int. Ed. 59 (2020) 4652–4669.

[58] N. Prasetya, B.P. Ladewig, An insight into the effect of azobenzene functionalities studied in UiO-66 frameworks for low energy CO_2 capture and CO_2/N_2 membrane separation, J. Mater. Chem. 7 (2019) 15164–15172.

[59] L.L. Dang, X.J. Zhang, L. Zhang, J.Q. Li, F. Luo, X.F. Feng, Photo-responsive azo MOF exhibiting high selectivity for CO_2 and xylene isomers, J. Coord. Chem. 69 (2016) 1179–1187.

[60] H. Li, M.R. Hill, C. Doblin, S. Lim, A.J. Hill, P. Falcaro, Visible light triggered CO_2 liberation from silver nanocrystals incorporated metal–organic frameworks, Adv. Funct. Mater. 26 (2016) 4815–4821.

[61] A. Knebel, L. Sundermann, A. Mohmeyer, I. Strauß, S. Friebe, P. Behrens, J. Caro, Azobenzene guest molecules as light-switchable CO_2 valves in an ultrathin UiO-67 membrane, Chem. Mater. 29 (2017) 3111–3117.

[62] K. Müller, J. Wadhwa, J.S. Malhi, L. Schöttner, A. Welle, H. Schwartz, D. Hermann, U. Ruschewitz, L. Heinke, Photoswitchable nanoporous films by loading azobenzene in metal–organic frameworks of type HKUST-1, Chem. Commun. 53 (2017) 8070–8073.

[63] J. Park, B.L. Suh, J. Kim, Computational design of a photoresponsive metal–organic framework for post combustion carbon capture, J. Phys. Chem. C 124 (2020) 13162–13167.

[64] V.V. Butova, O.A. Burachevskaya, V.A. Podshibyakin, E.N. Shepelenko, A.A. Tereshchenko, S.O. Shapovalova, O.I. Il'in, V.A. Bren', A.V. Soldatov, Photoswitchable zirconium MOF for light-driven hydrogen storage, Polymers 13 (2021) 4052.

[65] L. Zhang, L.L. Wang, L.L. Gong, X.F. Feng, M.B. Luo, F. Luo, Coumarin-modified microporous-mesoporous Zn-MOF-74 showing ultra-high uptake capacity and photo-switched storage/release of U^{VI} ions, J. Hazard Mater. 311 (2016) 30–36.

[66] Y. Dou, Y. Hu, S. Yuan, W. Wu, H. Tang, Detailed mechanism of *trans–cis* photoisomerization of azobenzene studied by semiclassical dynamics simulation, Mol. Phys. 107 (2009) 181–190.

[67] J. Griffiths, II. Photochemistry of azobenzene and its derivatives, Chem. Soc. Rev. 1 (1972) 481–493.

[68] M. Han, T. Honda, D. Ishikawa, E. Ito, M. Hara, Y. Norikane, Realization of highly photoresponsive azobenzene-functionalized monolayers, J. Mater. Chem. 21 (2011) 4696–4702.

[69] N. Liu, Z. Chen, D.R. Dunphy, Y.B. Jiang, R.A. Assink, C.J. Brinker, Photoresponsive nanocomposite formed by self-assembly of an azobenzene-modified silane, Angew. Chem. Int. Ed. 42 (2003) 1731–1734.

[70] A. Khayyami, A. Philip, M. Karppinen, Atomic/molecular layer deposited iron-azobenzene framework thin films for stimuli-induced gas molecule capture/release, Angew. Chem. Int. Ed. 58 (2019) 13400–13404.

[71] C.L. Jones, A.J. Tansell, T.L. Easun, The lighter side of MOFs: structurally photoresponsive metal–organic frameworks, J. Mater. Chem. 4 (2016) 6714–6723.

[72] X. Yu, Z. Wang, M. Buchholz, N. Füllgrabe, S. Grosjean, F. Bebensee, S. Bräse, C. Wöll, L. Heinke, *Cis*-to-*trans* isomerization of azobenzene investigated by using thin films of metal–organic frameworks, Phys. Chem. Chem. Phys. 17 (2015) 22721–22725.

[73] L.T.M. Hoang, L.H. Ngo, H.L. Nguyen, H.T.H. Nguyen, C.K. Nguyen, B.T. Nguyen, Q.T. Ton, H.K.D. Nguyen, K.E. Cordova, T. Truong, An azobenzene-containing metal–organic framework as an efficient heterogeneous catalyst for direct amidation of benzoic acids: synthesis of bioactive compounds, Chem. Commun. 51 (2015) 17132–17135.

[74] D. Hermann, H.A. Schwartz, M. Werker, D. Schaniel, U. Ruschewitz, Metal–organic frameworks as hosts for fluorinated azobenzenes: a path towards quantitative photoswitching with visible light, Chem. Eur J. 25 (2019) 3606–3616.

[75] J. Park, D. Yuan, K.T. Pham, J.R. Li, A. Yakovenko, H.C. Zhou, Reversible alteration of CO_2 adsorption upon photochemical or thermal treatment in a metal–organic framework, J. Am. Chem. Soc. 134 (2012) 99–102.

[76] A. Pianwanit, C. Kritayakornupong, A. Vongachariya, N. Selphusit, T. Ploymeerusmee, T. Remsungnen, D. Nuntasri, S. Fritzsche, S. Hannongbua, The optimal binding sites of CH_4 and CO_2 molecules on the metal–organic framework MOF-5: ONIOM calculations, Chem. Phys. 349 (2008) 77–82.

[77] J.R. Karra, K.S. Walton, Molecular simulations and experimental studies of CO_2, CO, and N_2 adsorption in metal–organic frameworks, J. Phys. Chem. C 114 (2010) 15735–15740.

[78] J.M. Knaust, S.W. Keller, A mixed-ligand coordination polymer from the *in situ*, Cu(I)-mediated isomerization of bis(4-pyridyl)ethylene, Inorg. Chem. 41 (2002) 5650–5652.

[79] S.S. Sun, J.A. Anspach, A.J. Lees, Self-assembly of transition-metal-based macrocycles linked by photoisomerizable ligands: examples of photoinduced conversion of tetranuclear-dinuclear squares, Inorg. Chem. 41 (2002) 1862–1869.

[80] A.O.T. Patrocinio, M.K. Brennaman, T.J. Meyer, N.Y.M. Iha, Excited-state dynamics in *fac*–$[Re(CO)_3(Me_4phen)(L)]^+$, J. Phys. Chem. 114 (2010) 12129–12137.

[81] A. Schaate, S. Dühnen, G. Platz, S. Lilienthal, A.M. Schneider, P. Behrens, A novel Zr-based porous coordination polymer containing azobenzenedicarboxylate as a linker, Eur. J. Inorg. Chem. (2012) 790–796, 2012.

[82] B. Chen, S. Ma, E.J. Hurtado, E.B. Lobkovsky, H.C. Zhou, A triply interpenetrated microporous metal–organic framework for selective sorption of gas molecules, Inorg. Chem. 46 (2007) 8490–8492.

[83] C.A. Bauer, T.V. Timofeeva, T.B. Settersten, B.D. Patterson, V.H. Liu, B.A. Simmons, M.D. Allendorf, Influence of connectivity and porosity on ligand-based luminescence in zinc metal–organic frameworks, J. Am. Chem. Soc. 129 (2007) 7136–7144.

[84] G. Socrates, Infrared and Raman Characteristic Group Frequencies: Tables and Charts, John Wiley & Sons, 2004.

[85] D. Feng, K. Wang, Z. Wei, Y.P. Chen, C.M. Simon, R.K. Arvapally, R.L. Martin, M. Bosch, T.F. Liu, S. Fordham, D. Yuan, M.A. Omary, M. Haranczyk, B. Smit, H.C. Zhou, Kinetically tuned dimensional augmentation as a versatile synthetic route towards robust metal–organic frameworks, Nat. Commun. 5 (2014) 5723.

[86] H.C. Zhou, J.R. Long, O.M. Yaghi, Introduction to metal–organic frameworks, Chem. Rev. 112 (2012) 673–674.

[87] R. Cheng, F. Meng, C. Deng, H.A. Klok, Z. Zhong, Dual and multi-stimuli responsive polymeric nanoparticles for programmed site-specific drug delivery, Biomaterials 34 (2013) 3647–3657.

[88] H. Li, M.M. Sadiq, K. Suzuki, R. Ricco, C. Doblin, A.J. Hill, S. Lim, P. Falcaro, M.R. Hill, Magnetic metal–organic frameworks for efficient carbon dioxide capture and remote trigger release, Adv. Mater. 28 (2016) 1839–1844.

[89] M.M. Sadiq, H. Li, A.J. Hill, P. Falcaro, M.R. Hill, K. Suzuki, Magnetic induction swing adsorption: an energy efficient route to porous adsorbent regeneration, Chem. Mater. 28 (2016) 6219–6226.

[90] S. Li, J. Hu, Photolytic and photocatalytic degradation of tetracycline: effect of humic acid on degradation kinetics and mechanisms, J. Hazard Mater. 318 (2016) 134–144.

[91] F. Bigdeli, C.T. Lollar, A. Morsali, H.C. Zhou, Switching in metal–organic frameworks, Angew. Chem. Int. Ed. 59 (2020) 4652–4669.

[92] A.L. Demain, Antibiotics: natural products essential to human health, Med. Res. Rev. 29 (2009) 821–842.

[93] R. Lyndon, K. Konstas, A.W. Thornton, A.J. Seeber, B.P. Ladewig, M.R. Hill, Visible light-triggered capture and release of CO_2 from stable metal–organic frameworks, Chem. Mater. 27 (2015) 7882–7888.

[94] J.D. Webb, H.H. Neidlinger, J.S. Connolly, An infrared study of azobenzene photoisomerization in a polymer matrix, Polym. Photochem. 7 (1986) 503–515.

[95] M. Kazuyuki, N. Takashi, Y. Tsutomu, S. Takeyuki, S. Takahiro, Reversible photoswitching liquid-phase adsorption on azobenzene derivative-grafted mesoporous silica, Chem. Lett. 35 (2006) 736–737.

[96] T. Tanaka, H. Ogino, M. Iwamoto, Photochange in pore diameters of azobenzene-planted mesoporous silica materials, Langmuir 23 (2007) 11417–11420.

[97] I.M. Walton, J.M. Cox, J.A. Coppin, C.M. Linderman, D.G.D. Patel, J.B. Benedict, Photo-responsive MOFs: light-induced switching of porous single crystals containing a photochromic diarylethene, Chem. Commun. 49 (2013) 8012–8014.

[98] L. Dong, Y. Feng, L. Wang, W. Feng, Azobenzene-based solar thermal fuels: design, properties, and applications, Chem. Soc. Rev. 47 (2018) 7339–7368.

[99] G. Kresse, J. Hafner, *Ab initio* molecular dynamics for open-shell transition metals, Phys. Rev. B 48 (1993) 13115–13118.

[100] G. Kresse, J. Furthmüller, Efficiency of *ab-initio* total energy calculations for metals and semiconductors using a plane-wave basis set, Comput. Mater. Sci. 6 (1996) 15–50.

[101] Z. Yi, J. Ye, N. Kikugawa, T. Kako, S. Ouyang, H. Stuart-Williams, H. Yang, J. Cao, W. Luo, Z. Li, Y. Liu, R.L. Withers, An orthophosphate semiconductor with photooxidation properties under visible-light irradiation, Nat. Mater. 9 (2010) 559–564.
[102] L. Luo, Y. Li, J. Hou, Y. Yang, Visible photocatalysis and photostability of Ag_3PO_4 photocatalyst, Appl. Surf. Sci. 319 (2014) 332–338.
[103] C. Mu, Y. Zhang, W. Cui, Y. Liang, Y. Zhu, Removal of bisphenol A over a separation free 3D Ag_3PO_4-graphene hydrogel via an adsorption-photocatalysis synergy, Appl. Catal. B Environ. 212 (2017) 41–49.
[104] Y. Bi, S. Ouyang, N. Umezawa, J. Cao, J. Ye, Facet effect of single-crystalline Ag_3PO_4 sub-microcrystals on photocatalytic properties, J. Am. Chem. Soc. 133 (2011) 6490–6492.
[105] W. Teng, X. Li, Q. Zhao, J. Zhao, D. Zhang, *In situ* capture of active species and oxidation mechanism of RhB and MB dyes over sunlight-driven Ag/Ag_3PO_4 plasmonic nanocatalyst, Appl. Catal. B Environ. 125 (2012) 538–545.
[106] G. Dai, J. Yu, G. Liu, A new approach for photocorrosion inhibition of Ag_2CO_3 photocatalyst with highly visible-light-responsive reactivity, J. Phys. Chem. C 116 (2012) 15519–15524.
[107] I. Rodrigues, I. Mihalcea, C. Volkringer, T. Loiseau, M. Visseaux, Water-free neodymium 2,6-naphthalenedicarboxylates coordination complexes and their application as catalysts for isoprene polymerization, Inorg. Chem. 51 (2012) 483–490.
[108] K. Yin, Q. Wang, M. Lv, L. Chen, Microorganism remediation strategies towards heavy metals, Chem. Eng. J. 360 (2019) 1553–1563.